Journal of the Meteorological Society of Japan, Vol. 74, No. 6, pp. 867–890, 1996

Tropical and Mid-latitude 45-Day Perturbations over the Western Pacific During the Northern Summer

By Ryuichi Kawamura,[1] Takio Murakami and Bin Wang

Department of Meteorology, School of Ocean and Earth Science and Technology, University of Hawaii, Honolulu, Hawaii

(Manuscript received 22 April 1996, in revised form 7 October 1996)

Abstract

The tropical Madden-Julian oscillation (MJO), which is of convective origin, systematically propagates northward in the Western North Pacific summer monsoon region (5°–20°N, 110°–160°E). The northward propagating MJO, which is statistically significant, displays strong horizontally and vertically asymmetric circulation. The low-level cyclonic response is pronounced due to the presence of convergent, cyclonically sheared mean monsoon flow, while the upper-level anticyclonic counterpart is weak due to the influence of the divergent, anticyclonically sheared upper-level mean monsoon flow. The upper tropospheric MJO response is largely associated with divergent winds, as manifested by strong equatorward outflows that export anticyclonic vorticity into the upper troposphere of the Southern Hemisphere. The summer mean monsoon flow is responsible for reinforcing the vertical asymmetry of the MJO circulation induced by convective heating, and for generating a barotropic component in the baroclinic MJO through the mean monsoon flow-MJO interaction.

The mid-latitude intraseasonal oscillation (ISO) displays a barotropic wave train structure along a great circle traversing the North Pacific, and exhibits the largest variability in the westerly jet exit region of the North Pacific (40°–50°N, 180°–150°W). This phenomenon is attributed to the combination of two different dynamic processes. While the MJO is propagating northward, the barotropic MJO component generated by the mean monsoon flow-MJO interaction produces a significant tropical-extratropical interaction on the intraseasonal time scale. Namely, when the 45-day convective activity becomes strongest near the Philippines, the barotropic MJO component acts as an origin of the barotropic Rossby wave dispersion emanating out of the convective forcing, eventually contributing to the development of an extratropical ISO. The enstrophy budget analysis shows, on the other hand, that the largest contribution to ISO is the *in situ* barotropic mean flow-ISO interaction in and around the jet exit.

1. Introduction

Madden and Julian (1971; 1972) discovered 30–60 day oscillations that are primarily associated with equatorial zonal wind perturbations with a wavenumber one and an out of phase relationship between the lower and upper tropospheres. For brevity, these tropical 30–60 day oscillations are hereafter termed as the "tropical MJO" (refer to the Appendix for symbols used). Yasunari (1980; 81) found a systematic northward propagation of the tropical MJO, which originates in the equatorial Indian Ocean. The northward passage of cloud bands is associated with an alternation between active and break monsoons over India (Sikka and Gadgil, 1980). Based on the 1978–79 FGGE/MONEX data, several authors (*e.g.*, Krishnamurti and Subrahmanyan, 1982; Lorenc, 1984; Murakami and Nakazawa, 1985) further documented the linkage between the Southeast Asia summer monsoon (SEAM) and the eastward- as well as northward-migrating MJO. Using a zonally symmetric, non-linear, two-layer model containing an interactive ocean and a continent poleward of 18°N, Webster and Chou (1980) emphasized the importance of a full hydrology cycle at the land surface for the northward migration of simulated intraseasonal perturbations with periods of about 15 days. Goswami and Shukla (1984) found that northward-moving perturbations, appearing in their zonally symmetric GCM, are maintained by the latent heat of evaporation from the surface. Lau and Chan (1986) presented the possibility that the meridional propagation of MJO comes from a result of the interaction between the

1 On leave from the National Research Institute for Earth Science and Disaster Prevention, Tsukuba, Japan

©1996, Meteorological Society of Japan

monsoon circulations and MJO disturbances.

On the other hand, the tropical MJO has been viewed as a global-scale eastward-propagating mode along the equator (*e.g.*, Knutson and Weickmann 1987; Hendon and Liebmann, 1994; Hendon and Salby, 1994). Numerical simulations with various versions of GCMs have also reproduced eastward-propagating tropical MJO (*e.g.*, Hayashi and Sumi, 1986; Lau and Lau, 1986; Lau *et al.*, 1988). Despite their composite analysis based on the eastward-propagating mode on a global scale, Knutson and Weickmann (1987) also showed a northward-propagating feature of MJO, especially over the western Pacific in boreal summer. Wang and Rui (1990) documented, based on pentad-mean OLR data, that there are two types of the northward-propagating MJO over the western Pacific: one is the mode intimately associated with an equatorial eastward-propagating mode and the other is the independent northward-propagating mode. They also mentioned that about one half of the northward-propagating MJO are not related to the equatorial eastward-propagating mode. Their result suggests that there is another mechanism for the origin of the northward-propagating MJO. Thus, if we highlight MJO disturbances over the western Pacific monsoon region in boreal summer, a composite analysis based on the northward-propagating mode should be made to exactly extract its dynamical structure.

Since the MJO convective disturbances are prominent in the western Pacific, it is expected that there are strong interactions between the western Pacific monsoon circulation (*e.g.*, Holland, 1995) and the northward-propagating MJO (*e.g.*, Murakami, 1984; Murakami *et al.*, 1986; Chen and Murakami, 1988). However, it is still uncertain how the monsoon circulation interacts with MJO disturbances. The mean monsoon flow, which is convergent (divergent) and cyclonically (anticyclonically) sheared in the lower (upper) troposphere, appears to exert a strong measure of control upon determining the vertical structural features of convection-induced MJO. One example is the vertical asymmetry in the MJO-related anomalous divergence field; namely, stronger upper-level divergence as compared with weaker low-level convergence. This statement can be justified from indirect observational evidence provided by Madden (1986) and Hendon and Liebmann (1994) that the MJO-related cross-equatorial flow of essentially divergent character is much more prominent in the upper than in the lower troposphere. We found, on the other hand, that the mean monsoon flow - MJO interaction brings about a vertical asymmetry in the convection- induced MJO vorticity in such a way that the lower tropospheric cyclonic vorticity is much stronger than its upper tropospheric anticyclonic counterpart. This will be shown in Section 3.

Another major concern is the extratropical intraseasonal variations prevailing over the North Pacific region. Krishnamurti and Gadgil (1985) found a strong signal of intraseasonal variability with an approximate period of 45 days in mid-latitude regions, which is nearly in phase in the vertical (*i.e.*, barotropic), and most prominent in and around the westerly jet stream. Using a singular spectrum analysis, Ghil and Mo (1991) detected a 48-day mode prevailing in the northern extratropics. Their studies thus show that the extratropical 40–50 day oscillating mode is significant and not an artifact of the analysis. Furthermore, they mentioned that there are no significant correlations between tropical MJO and extratropical intraseasonal modes in boreal summer. Knutson and Weickmann (1987) also demonstrated that the extratropical response to anomalous convection associated with MJO in the summer hemisphere was not statistically significant. Yet, Murakami (1987), who investigated the MJO related, tropical-extratropical teleconnection during boreal summer, found a series of time-clustered, space-overlapping disturbance developments, similar to what is generally referred to as the Rossby wave dispersion. Magana and Yanai (1991) showed that the tropical upper tropospheric trough (TUTT) acts as a westerly duct for penetration, thus allowing wave energy to propagate equatorward as well as poleward in terms of the tropical-extratropical interaction. Over the western Pacific, on the other hand, a summertime extratropical wave train associated with anomalous convection around the Philippines is demonstrated by Nitta (1987), and Huang and Li (1987). Very recently, Wang and Xie (1996) investigated the mechanisms through which a sheared basic flow affects tropical waves, using a two-level equatorial β-plane model. They demonstrated that the prominence of vertical shear is a necessary condition for internal heat-induced equatorial Rossby waves to penetrate into the extratropics by transforming their structures from baroclinic to barotropic in the vertical. Furthermore, since the tropical MJO tends to migrate northward over the western Pacific, its northward propagation may make it easy to interact between tropical and extratropical atmospheres in terms of the MJO time scale. Thus, the issue on the summertime tropical-extratropical interaction with the MJO time scale should be further investigated precisely because two different conclusions are given.

In the present study we investigate to what extent and how the three-dimensional shear of the climatological summer mean flow affects the tropical MJO as well as the mid-latitude intraseasonal oscillation. Sections 3 and 4 present evidence of the mean flow influence upon MJO, focusing specifically on the northward-propagating tropical MJO. The mid-latitude intraseasonal oscillation is also regulated by the three-dimensional shear of the summer-

Table 1. Weight function of the low-pass time filter used in this study.

k	0	±1	±2	±3	±4	±5
w_k	0.14210	0.13567	0.11742	0.09030	0.05856	0.02700

time mean westerly jet. In Section 5 we explore why the mid-latitude intraseasonal oscillation becomes most pronounced in the Pacific jet exit region. The possible link between the barotropic mid-latitude intraseasonal oscillation and the barotropic as well as baroclinic tropical MJO of convective origin is examined in Section 6.

2. Data and analysis procedures

2.1 Definition of MJO and high-frequency transient components

Datasets used in this study include: (1) infrared equivalent blackbody temperature (T_{BB}) derived from the Japanese Geostationary Meteorological Satellite, and (2) u, v, T, ϕ and q extracted from the ECMWF (European Centre for Medium-Range Weather Forecasts) gridded global analysis with a spatial resolution of 2.5° × 2.5° from 10°S to 60°N and between 60°E and 140°W, for the period of 1985–93. During this period, the ECMWF analysis and initialization schemes remained practically unchanged, thus providing datasets of nearly uniform quality.

A series of daily data for n years is signified as A_i, $i = 1$ to $365n$. A low-pass time filter is then applied to A_i as follows:

$$\overline{A}_i = \sum_{k=-5}^{+5} w_k A_{i-k}, \quad i = 1 \text{ to } 365n,$$

where the weights w_k are given in Table 1. The response is approximately 0.2 for a 10-day period and zero for transients with periods of less than 8 days. Introducing a prime to define a departure of A_i from its mean $\overline{A}_i$:

$$A'_i = A_i - \overline{A}_i,$$

where A'_i represents transient variability with periods shorter than approximately 15 days. In Section 5, A'_i is considered in evaluating a non-linear barotropic interaction between MJO and short-period transient components. Within the scope of the present study, a simple representation of transients by A'_i and $\overline{A}_i$ appears to be adequate.

To extract the MJO component, we applied the band-pass time filter as proposed by Shanks (1967) to the daily data of $\overline{A}_i$ by choosing $\omega_0 = 2\pi/45$ days and $\omega_1 = 2\pi/20$ days, so that the maximum response of about 1.0 is obtained at 45 days, while oscillations shorter (longer) than 30 (90) days are satisfactorily reduced to less than 50 %. We, therefore, refer to the extracted data ($\tilde{A}$) as the MJO component. It should be noted that the time filter used is also useful for detecting adequately the extratropical 40–50 day oscillation (signified as "mid-latitude ISO").

Our focus is on the time series of $\tilde{A}$ only during the boreal summer from Pentad 31 (May 31–June 4) to Pentad 53 (September 18–22) of each year when the western North Pacific monsoon (WNPM) prevails. Each boreal summer has about 3 cycles of MJO, on average. The climatological summer mean, which is denoted as $\langle A \rangle$, is defined by the n-year mean of $\overline{A}$ from P31 to P53. We find it interesting to evaluate the variance of $\tilde{A}$, *i.e.*, $\left\langle \tilde{A}^2 \right\rangle$, as an indicator of MJO activities during boreal summer. Here, A can be any meteorological variable, including T_{BB}, u, v, T, ϕ and q.

Although previous studies already indicated the existence of mid-latitude ISO (Krishnamurti and Gadgil, 1985; Ghil and Mo, 1991), we will confirm, here, whether the summertime mid-latitude ISO over the North Pacific is really significant. Figure 1 shows the time-longitude section of the ratio of 30–90 day kinetic energy to the total transient eddy kinetic energy with periods shorter than about 90 days, computed at 35°–45°N, corresponding to the westerly jet of the North Pacific. Both 850-hPa and 200-hPa levels are considered in computing the ratio. At 850 hPa, the jet exit region around 180°–140°W is characterized by the dominance of high ratios exceeding 30 %, especially from late June to mid-September. Similarly, high-ratio areas are observed in boreal summer at the upper level. The above results certainly indicate that the mid-latitude ISO stands out high above the noise level and is significant during boreal summer.

2.2 Summer monsoon climatology

The climatological summer mean winds at 850 and 200 hPa are shown in Figs. 2a and 2b, which are compared with the variance of relative vorticity $\tilde{\zeta}_{850}$ and $\tilde{\zeta}_{200}$ presented in Figs. 2c and 2d. The confluence zone (5°–30°N, 110°–150°E) between the SEAM monsoon westerlies and the North Pacific trades is characterized by a strong variability of $\tilde{\zeta}_{850}$. The variance of $\tilde{\zeta}_{850}$ is significantly large over the SEAM domain (Arabian Sea - Bay of Bengal) where the climatological low-level westerlies are dominant. In contrast, the easterly trades over the North Pacific strongly depress the variance of $\tilde{\zeta}_{850}$. Large variability in $\tilde{\zeta}_{850}$ is also found in the westerlies north of the subtropical ridge in the western North

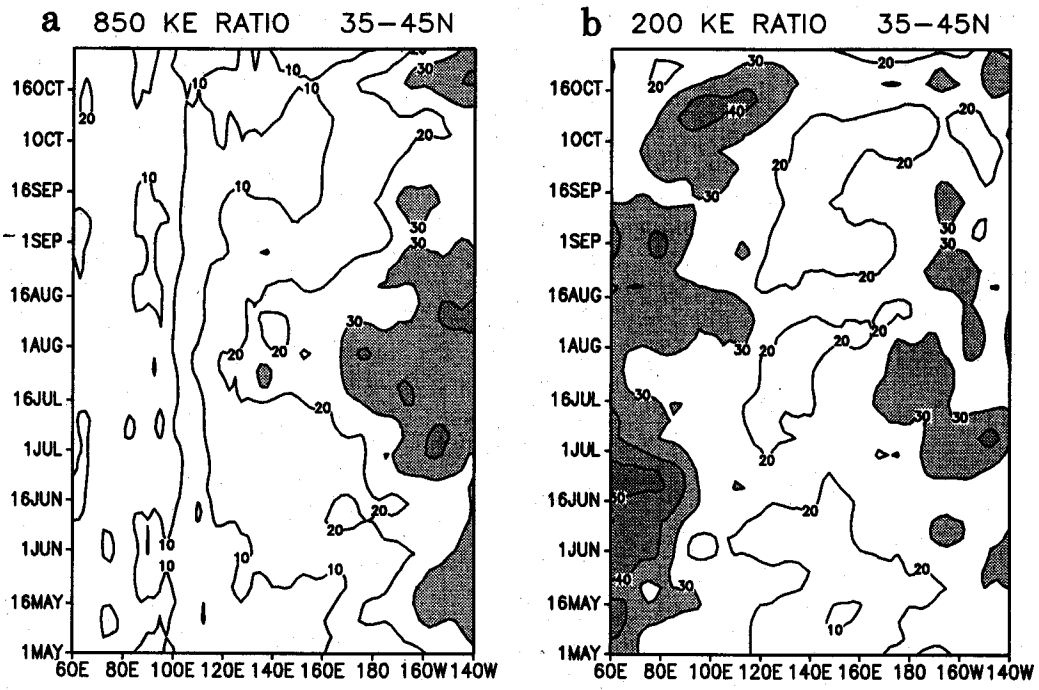

Fig. 1. Time-longitude sections of the ratio (percentage) of 30–90 day kinetic energy to the total transient eddy kinetic energy with periods shorter than 90 days, along 35°–45°N at 850 hPa (a) and 200 hPa (b). Contour intervals are 10 % and shading indicates regions of greater than 30 %.

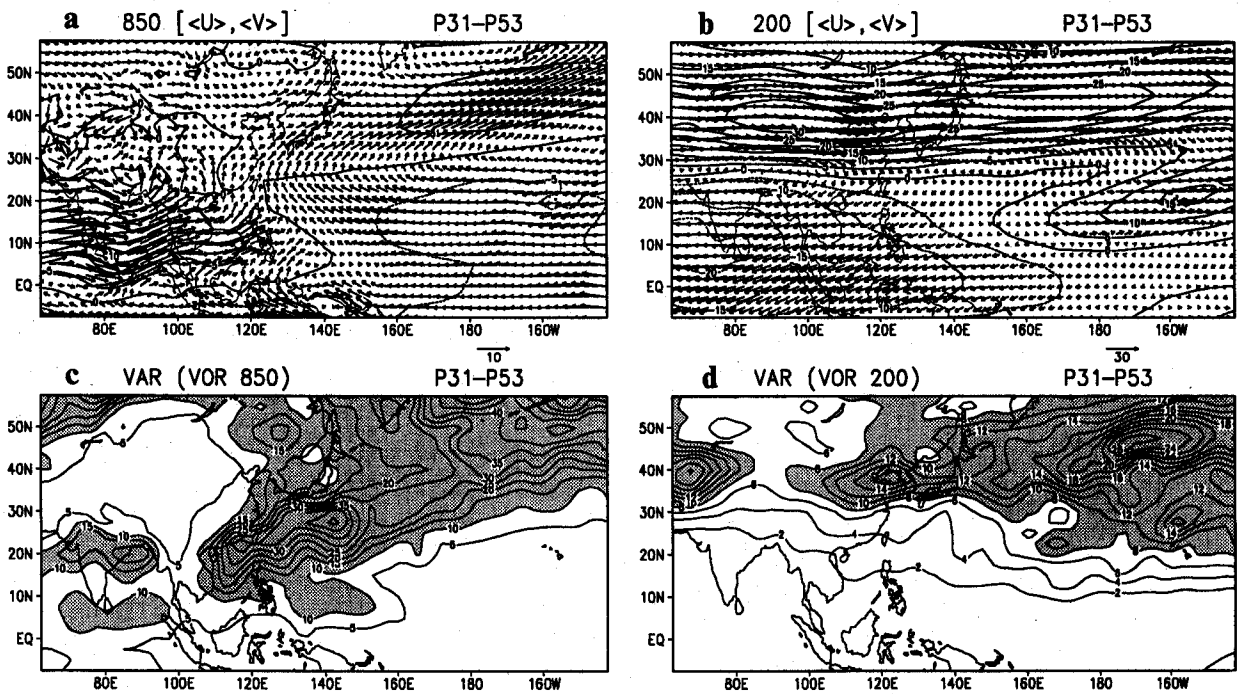

Fig. 2. Climatological summer mean winds at 850 hPa (a) and 200 hPa (b), averaged between pentads 31 (May 31–June 4) and 53 (September 18–22) during the 9 yr 1985–93. The interval of isotachs of zonal wind is 5 ms^{-1}. The variance of 45-day filtered vorticity at 850 hPa (c: units are 10^{-12} s^{-2}; the interval is 5 units) and 200 hPa (d: units are 10^{-11} s^{-2}; the interval is 2 units). Shading indicates regions of greater than 10 (8) units at 850 (200) hPa.

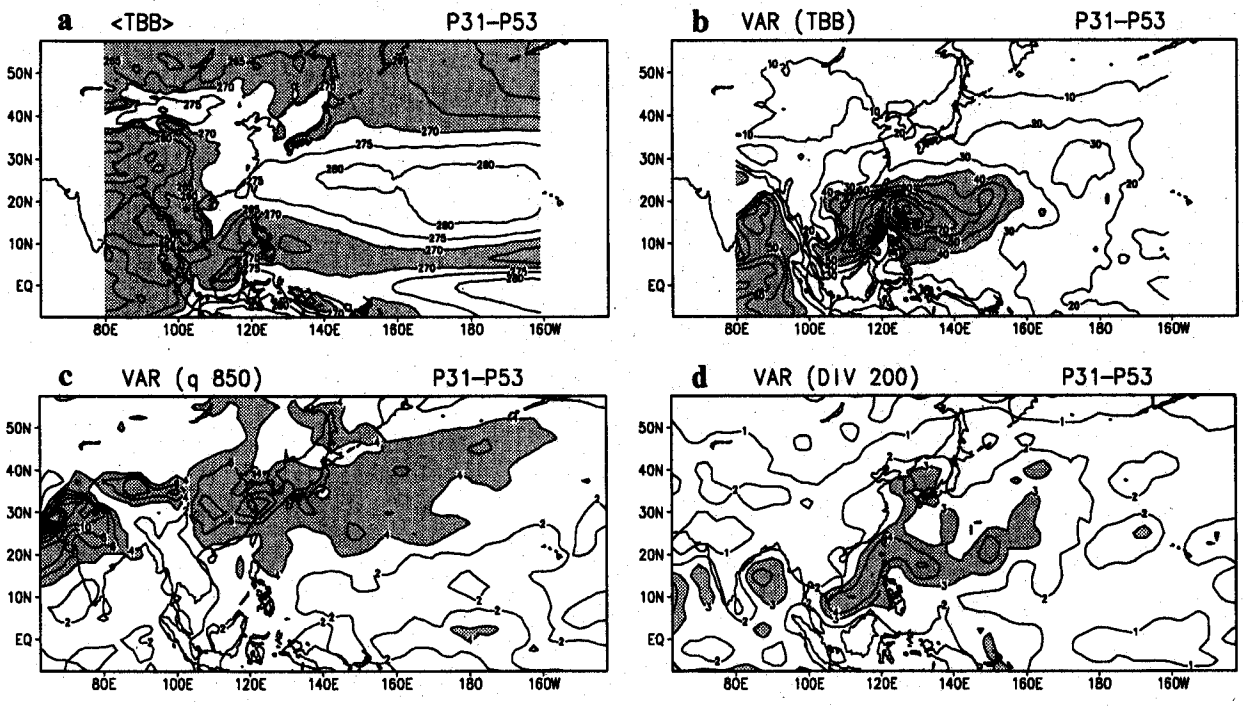

Fig. 3. (a) Climatological summer mean $\langle T_{BB} \rangle$ (the interval is 5 K; shading is for less than 270 K). (b) Variance of $\tilde{T}_{BB}$ (the interval is 10 K^2; shading is for greater than 40 K^2). (c) Variance of low-level specific humidity $\tilde{q}_{850}$ (the interval is 2×10^{-1} g^2 kg^{-2}; shading is for larger than 4×10^{-1} g^2 kg^{-2}). (d) Variance of upper-level divergence $\tilde{D}_{200}$ (the interval is 1×10^{-12} s^{-2}; shading is for greater than 3×10^{-12} s^{-2}).

Pacific.

At 200 hPa, we also see strong activities of mid-latitude ISO dominating along the westerly jet axis. The climatological jet stream considerably weakens to the east of the dateline along about 45°N. This jet exit is highlighted by the strongest $\tilde{\zeta}_{200}$ variance during boreal summer. Equatorward of the jet exit is the zonally extended TUTT with the tropical westerlies to its south. There is a distinct zonal asymmetry between these tropical westerlies with substantial $\tilde{\zeta}_{200}$ variance and the monsoonal easterlies with much depressed $\tilde{\zeta}_{200}$ activities over the SEAM and WNPM domain.

The climatological summer mean $\langle T_{BB} \rangle$ is lowest over the key area of SEAM, *i.e.*, central India and the eastern Bay of Bengal (Fig. 3a), while the variance of $\tilde{T}_{BB}$ is strongest in the midst of the monsoon domain around 20°N, 130°E (Fig. 3b). As far as the 45-day variations are concerned, WNPM turns out to be more violent than SEAM. The variance of $\tilde{T}_{BB}$ is quite small outside of the monsoon domain. An immediate inference is that the mid-latitude ISO identified in Figs. 2c and 2d is not of convective origin. Its development, however, is likely regulated, in some way, by convectively induced tropical MJO. This possibility will be examined later.

The monsoon domain is characterized by a contrast between small variance of low-level specific humidity $\tilde{q}_{850}$ (Fig. 3c) and large variance of upper-level divergence $\tilde{D}_{200}$ (Fig. 3d). This means that the 45-day monsoonal convective oscillations are largely controlled by divergence fluctuations, rather than by moisture variations. At any rate, the variance of $\tilde{D}_{200}$ is well correlated with the $\tilde{T}_{BB}$ variance field, indicating that the ECMWF wind data are of good quality and can be utilized as the basic dataset for describing the nature of MJO.

Yet another feature of interest in Fig. 3d is the existence of relatively large $\tilde{D}_{200}$ variance within the confluence zone. Most probably, this is indicative of a northward migration of $\tilde{D}_{200}$ (or $\tilde{T}_{BB}$) perturbations through the confluence zone of climatological low-level southerly flow (Fig. 2a). A quick look at the time series of $\tilde{T}_{BB}$ confirms that such northward migration is common to any summer, as exemplified in Fig. 4 for the time series of $\tilde{T}_{BB}$ during the 1990 and 1991 summers. There exists a distinct northward propagation of $\tilde{T}_{BB}$ perturbations from the equator to about 25°N. The northward propagation suddenly collapses after crossing over the western Pacific subtropical ridge line (Fig. 2a). At the same time, MJO changes its structure to non-divergent (see Fig. 3d). This is probably a manifestation of transition from the northward-moving, convectively induced tropical MJO to the non-divergent, mid-latitude ISO. Statistically, the northward progres-

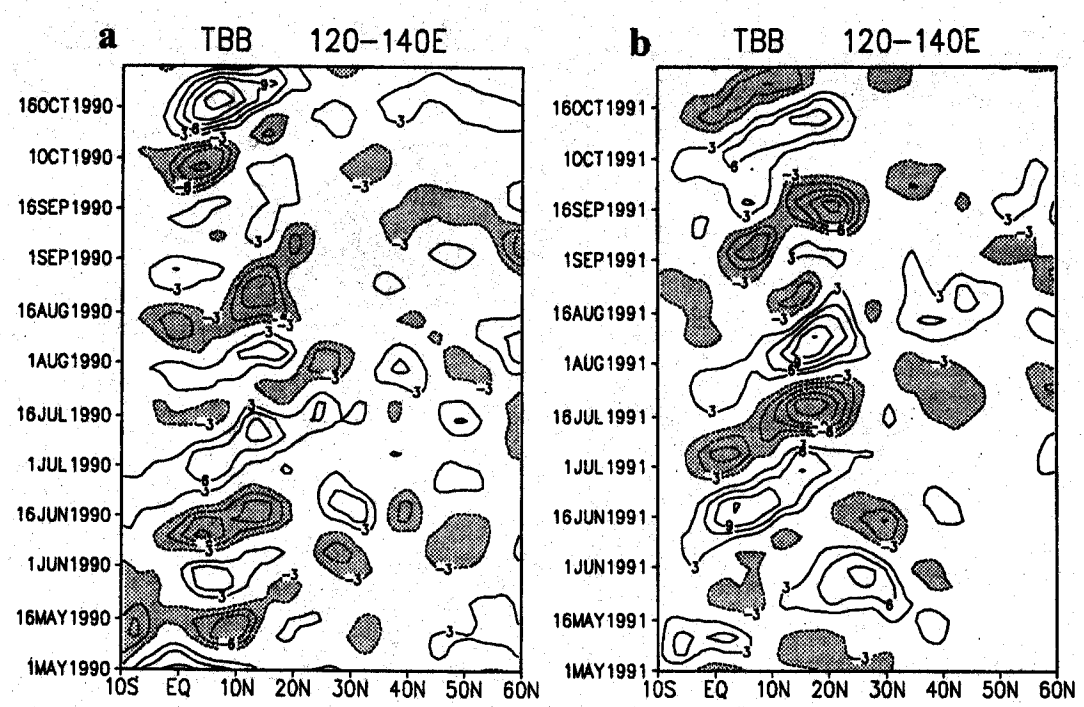

Fig. 4. Time-latitude sections of $\tilde{T}_{BB}$ averaged between 120° and 140°E during the summer (May 1–October 31) of 1990 (a) and 1991 (b). Contour intervals are for 3 K (no zero line) with dashed lines for less than −3 K.

sion can be seen during more than 80 % of the total observing period of the 1985–93 summers. Thus, the northward-propagating MJO unique to the confluence zone is statistically significant and can be used as an optimum reference for further investigation into the nature of MJO elsewhere.

2.3 Procedure of composite analysis

An empirical orthogonal function analysis was applied to pentad-mean $\tilde{T}_{BB}$ data, zonally averaged from 110° to 160°E at every 2 degrees of latitude from the equator to 30°N, for the period of 1985–93. Namely, the confluence zone was selected as the key area for the EOF analysis of northward-propagating MJO. The first four eigenvectors E_i (i = 1 to 4) are found to be significant by the sampling error test of North *et al.* (1982). As shown in Fig. 5, the fractional contribution of E_1 (E_2) to the total variance is 36 (30) %. Here, E_1 actually defines two anomalous patterns since its coefficient $c_1(t)$ may be either positive or negative. If $c_1(t)$ is negative on the n-th pentad, the sign of $c_1(t)E_1$ is negative near 4°N (above-normal convection), while it is positive at 22°N (below-normal convection). A similar argument also applies to the product of $c_2(t)E_2$.

The next step is to assign categories 1 to 9 with reference to $c_1(t)$ and $c_2(t)$. Category 1 is assigned to pentads at which $c_1(t)$ becomes minimum, while Category 5 is defined to pentads of maximum $c_1(t)$. Likewise, Category 3 (7) refers to pentads of minimum (maximum) $c_2(t)$. The remaining Categories

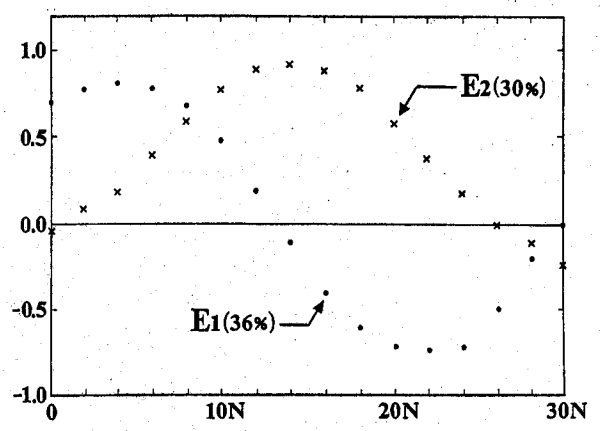

Fig. 5. The first (E_1) and second (E_2) eigenvector (non-dimensional) of EOF analyses of $\tilde{T}_{BB}$ averaged between 110° and 160°E from the equator to 30°N during boreal summer (Pentads 31–53) of 1985–93. See text for further information.

2, 4, 6 and 8 occupy intermediate $c_1(t)$ and $c_2(t)$ phases. Category 9 is identical to Category 1. During one cycle from Category 1 to 9, regions of active convection propagate northward from about 4°N to 30°N. For any variable, category values are evaluated with reference to the same selected pentads as determined from the $c_1(t)$ and $c_2(t)$ coefficients. This allows us to compare the category mean val-

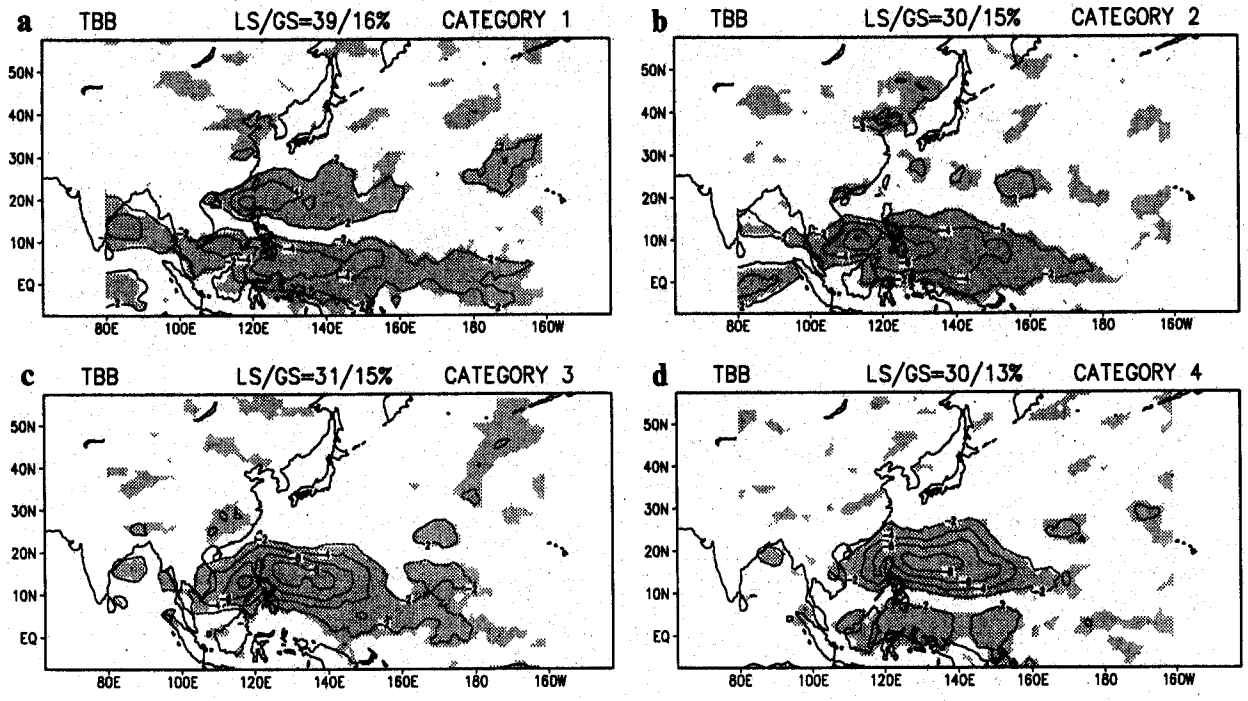

Fig. 6. Composite $\tilde{T}_{BB}$ maps at Categories 1 (a) to 4 (d). Contour intervals are for 2 K with negative contours dashed (no zero line). Shading indicates regions where the composite anomalies satisfy the 95 % local significant test. LS and GS values are shown at the top of each composite map. Refer to the text for additional information.

ues of different variables at different locations and different levels.

Because of the monitoring procedures described above, composite maps for any quantity in Categories 5 to 8 are nearly identical, except for a change of sign, to those for Categories 1 to 4. The local statistical significance of the difference between the mean composite values (an average of about 26 cases) for Categories i and $i+4$ ($i = 1$ to 4) was tested by the procedure described by Panofsky and Brier (1958). The areal percentage that surpasses the local 95 % confidence level is signified as "LS". It turns out that LS differs from one category to another, as well as from one variable to another. In order to further test the statistical significance of the difference between the two composite maps, a Monte Carlo simulation method was applied to approximate the probability density function of the areal percentage that is statistically significant at the 95 % local confidence level (refer to Livezey and Chen, 1983). The statistically significant percentage area is denoted as "GS". A composite map is considered to be really significant if LS for this particular composite map is greater than GS. Thus, our composite analysis is tested in terms of both local and field significance. As will be shown later, this criterion is met for all composite maps to be presented in this paper.

To test whether the composite maps are reproducible or not, different composites were constructed with reference to EOF analyses of $\tilde{T}_{BB}$ at different locations, such as the equatorial Indian Ocean near 80°E, and the western North Pacific near 15°–20°N, 120°–140°E, where the variance of $\tilde{T}_{BB}$ is highest (Fig. 3b). Next, the $c_1(t)$ and $c_2(t)$ data were randomly grouped into six summers, followed by compositing for each group. Similar composite patterns emerged through these tests. An additional test was also made by computing one-point lag correlations for $\tilde{T}_{BB}$ (or $\tilde{\zeta}_{850}$, $\tilde{\zeta}_{200}$) with respect to the reference point at 15°N, 130°E (or 45°N, 160°W). These correlation patterns are also similar to the composite fields (not shown).

3. Composite MJO patterns

Figure 6 presents composite maps of $\tilde{T}_{BB}$ from Categories 1 to 4, all of which are statistically significant (*i.e.*, LS>GS). These maps provide useful information on the evolution of convection associated with the tropical MJO. [To save space, the composite maps for Categories 5 to 8 are not reproduced here.] The Category-1 pattern exhibits an active convective zone extending east-southeastward from southern India to as far east as the equatorial central Pacific. This category corresponds to the most active monsoon phase over southern India. Between Categories 1 and 3, the elongated convective zone with ESE-WNW tilt propagates north-

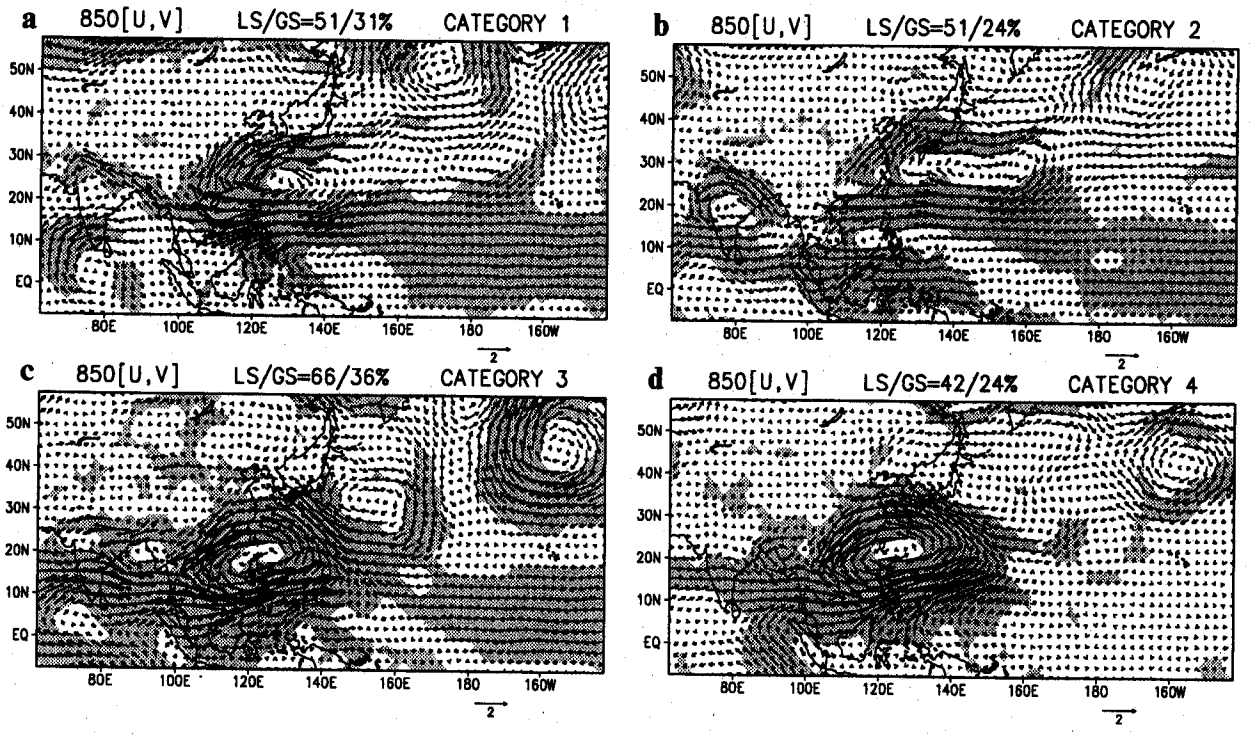

Fig. 7. As in Fig. 6, except for composite ($\tilde{u}_{850}$, $\tilde{v}_{850}$) winds (reference arrow: 2 ms^{-1}).

ward. This feature is already presented by previous studies (*e.g.*, Madden, 1986; Knutson and Weickmann, 1987; Hendon and Liebmann, 1994). Associated with this northward migration is the occurrence of a most-active monsoon just east of the Philippines with the lowest $\tilde{T}_{BB}$ of less than −8 K at Category 3 or 4. Between Categories 5 and 6 (same patterns as the Category 1 and 2, except for reversed signs), negative $\tilde{T}_{BB}$ perturbations continue to migrate northward, being dissipated after arriving at the northern most latitude of 25°–30°N after Category 6. At Category 5, a newly-born convective zone overlies the equatorial region of the Bay of Bengal which then propagates eastward, while intensifying, to the equatorial western Pacific by Category 8. This completes one cycle of convectively activated MJO, which brings about the active monsoons of SEAM and WNPM with certain regional phase lags. The above basic features are in agreement with those of Lau and Chan (1986).

Over the monsoon domain, convection is the major regulator of the wind variability at both 850 hPa (Fig. 7) and 200 hPa (Fig. 8). Between Categories 8 and 1, near-equatorial convection is strongest over the Borneo-New Guinea region. This near-equatorial convection enhances an eastern Kelvin wave response with anomalous easterlies (westerlies) to the east of about 150°(120°)E along the equator at 850 (200) hPa. At upper levels, the existence of positive height anomalies accompanied by anomalous westerlies (figure not shown) also supports the Kelvin wave explanation. After Category 3, the eastern Kelvin-wave response quickly shifts eastward and disappears. No Kelvin-wave response occurs when convection moves away from the equator. Such asymmetric heat sources with respect to the equator tend to excite a Rossby-wave response to its west. At Category 3, a dominant cyclonic circulation at 850 hPa is capped by a somewhat diffused anticyclonic circulation at 200 hPa. The dominant cyclonic circulation reflects dominance of a rotational part of the winds at 850 hPa. An exceptionally strong equatorward outflow at 200 hPa is noteworthy, as is also shown by Madden (1986), and Hendon and Liebmann (1994). This means that the upper-tropospheric response is characterized by a strong divergent component of the winds. In Fig. 8c, the poleward upper outflow is much weaker and less organized. This poleward outflow is circling along the eastern periphery of an anomalous cyclonic cell over the Tibetan Plateau. Namely, the Tibetan anticyclone (Fig. 2b) becomes weaker than normal at Category 3, which coincides with an initiation of the break monsoons over northern India - central China with a positive $\tilde{T}_{BB}$ anomaly (Fig. 6c) and an anomalous anticyclonic cell (although weak) at 850 hPa (Fig. 7c). A half cycle later, at Category 7, the monsoon refreshes, as active convection revives over the northern India - central China. At Category 1, a low-level anomalous anticyclonic cell centered around Taiwan provides northeasterly anomalies intruding into the Tropics. The anomalous northeast-

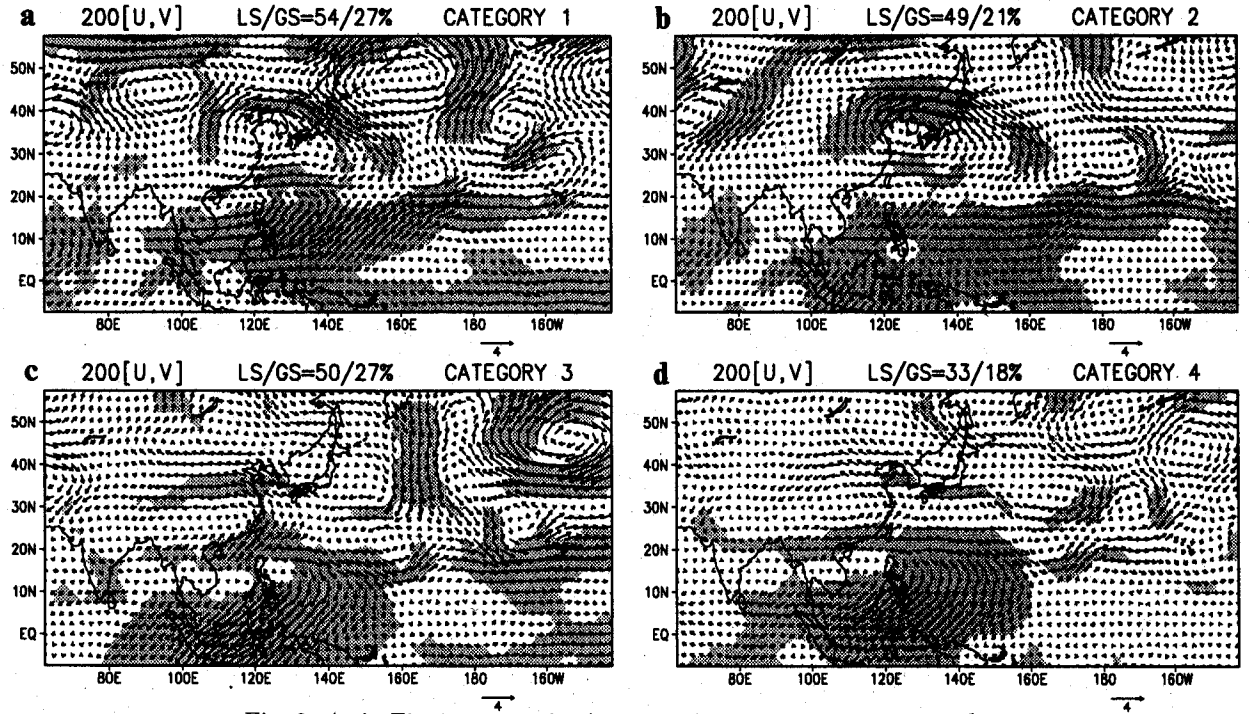

Fig. 8. As in Fig. 7, except for $(\tilde{u}_{200}, \tilde{v}_{200})$ winds in units of 4 ms^{-1}.

erlies are supposed to play an influential rôle in enhancing forthcoming convective perturbations.

No significant $\tilde{T}_{BB}$ perturbations occur at the mid-latitudes. The mid-latitude ISO exhibits a barotropic structure. At Category 3 (Figs. 7c and 8c), for example, we see vertically in-phase anticyclonic cells located at 47°N, 160°W at both 850 and 200 hPa. This anticyclone is replaced by a vertically coherent cyclonic cell by Category 7.

Our attention is next focused on the vorticity and divergence patterns at Category 3 shown in Fig. 9. The ζ_{850} pattern shows a distinct wave train emanating out of the convective center with two embedded cyclonic cells (signified as C_1 and C_2) and two anticyclonic cells (marked as A_1 and A_2) alternating approximately along a great circle with an average wavelength of 5,000 km. As stated earlier, A_2 is in phase with a similar anticyclonic vorticity cell at 200 hPa. Curiously, the associated divergence is near zero at both levels (Figs. 9b and 9d). Likewise, C_2 is also a non-divergent, barotropic disturbance. This is contrasted with the distinctly baroclinic vertical structure of C_1, which is centered to the northwest of intense convection. Namely, C_1 is of convective origin, forced by strong low-level convergence. Superimposed upon C_1 is the 200-hPa anticyclonic cell that is excited by convectively induced upper-level divergence. A_1 is featured by a transition from a baroclinic to a barotropic structure.

Some of the intriguing features of the vorticity and divergence fields near the Philippines at Category 3 are highlighted as follows: First, the magnitude of upper-level divergence is more than twice as large as that of low-level convergence. Second, the upper-level anticyclonic vorticity is, to our surprise, much weaker than the low-level cyclonic counterpart. Third, the upper-level anticyclonic center is displaced some two to three degrees of latitude equatorward of the convective center, while the low-level cyclonic center shifts slightly poleward.

To further investigate the relationship between $\tilde{\zeta}$ and $\tilde{D}$, we apply the 45-day filtering to each term in the vorticity equation. The resulting equation with frictional dissipation omitted can be written as

$$\frac{\partial \tilde{\zeta}}{\partial t} = \underset{A}{-\langle \boldsymbol{v} \rangle \cdot \nabla \tilde{\zeta}} \underset{B}{- \tilde{\boldsymbol{v}} \cdot \nabla \langle \eta \rangle} \underset{S_1}{- \langle \eta \rangle \tilde{D}} \underset{S_2}{- \tilde{\zeta} \langle D \rangle} \underset{N}{- \nabla \cdot \zeta' \tilde{\boldsymbol{v}}'}, \quad (1)$$

where $\eta = f + \zeta$. Equation 1 is equivalent to the 45-day filtered momentum equations derived by Murakami *et al.* (1984). In Eq. (1), the term A signifies the advection of $\tilde{\zeta}$ by the summer mean basic flow, while the term B describes the advection of $\langle \eta \rangle$ due to 45-day filtered winds. The so-called β-effect, *i.e.*, $-\beta\tilde{v}$, probably contributes most to B. The stretching term $S1$ is proportional to $\langle \eta \rangle$, which is substantially larger at 850 hPa than at 200 hPa due to the difference in horizontal shear of the summer mean monsoon flow between the two levels (see Fig. 2). The additional stretching term $S2$ is also regulated by the sheared mean monsoon flow, since $\langle D \rangle$ is strongly convergent at 850 hPa, while divergent at 200 hPa. Finally, the term N

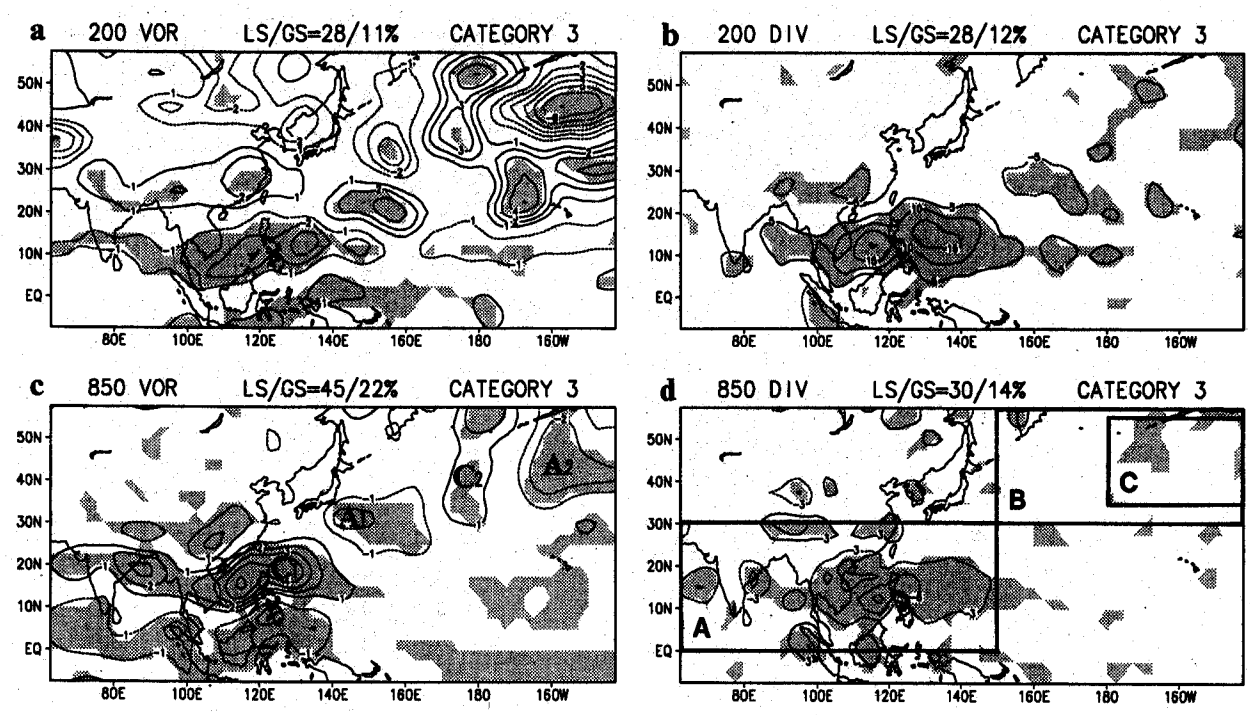

Fig. 9. Composite maps at category 3 for $\tilde{\zeta}_{200}$ (a; the interval is 1×10^{-6} s^{-1}), $\tilde{D}_{200}$ (b; the interval is 5×10^{-7} s^{-1}), $\tilde{\zeta}_{850}$ (c; the interval is 1×10^{-6} s^{-1}), and $\tilde{D}_{850}$ (d; the interval is 3×10^{-7} s^{-1}). Shading indicates regions surpassing the 95 % local significant test. Major cyclonic and anticyclonic disturbances at 850 hPa are marked by C_i and A_i ($i = 1,2$) which are approximately aligned along a great circle. Also shown are the regions A, B and C over which Eq. (2) was applied.

Table 2. Mean values of $\langle\zeta\rangle$, $\langle D\rangle$, $\tilde{\zeta}$ and $\tilde{D}$ (unit; 10^{-6} s^{-1}), and each term (unit; 10^{-11} s^{-2}) of Eq. (1) averaged over a region (5°–25°N, 110°–140°E) in Category 3.

Level	$\langle\zeta\rangle$	$\langle D\rangle$	$\tilde{\zeta}$	$\tilde{D}$	A	B	$S1$	$S2$	N	SUM
850	2.9	−2.8	3.2	−0.6	0.2	−0.8	2.4	0.7	−0.2	2.3
200	−6.5	2.9	−1.5	1.2	0.8	1.1	−3.7	0.4	0.1	−1.3

describes the non-linear barotropic interaction of $\tilde{\zeta}$ with transient eddies with periods shorter than about 15 days. The 45-day filtered transient eddy vorticity flux, $\widetilde{\zeta' v'}$, indicates the 45-day filtering of daily $u'\zeta'$and $v'\zeta'$vorticity transports. Although not explicitly included, Eq. (1) involves a residual term R, representing the 45-day filtering of $-\nabla\tilde{v}\tilde{\zeta}$. If $\tilde{v}$ and $\tilde{\zeta}$ oscillate with the same frequency $\omega_0 = 2\pi/45$ days, R becomes exactly zero. In reality, however, $\tilde{v}$ and $\tilde{\zeta}$ cover a wide frequency band from $2\pi/30$ days to $2\pi/90$ days and, hence, R does not vanish. Nevertheless, R is omitted in Eq. (1) since it is not important when considering the relationship between $\tilde{\zeta}$ and $\tilde{D}$. Also omitted in Eq. (1) is the 45-day filtering of non-linear products $v'\tilde{\zeta}$, $\tilde{v}\zeta'$, $\zeta'\tilde{D}$, and $\tilde{\zeta}D'$. This can be justified because of a little overlapping between spectra of the two variables under consideration.

Table 2 presents computed results of each term in Eq. (1), averaged from 5° to 25°N and between 110° and 140°E, the key area of active convection at Category 3 (Fig. 6c). Although the magnitude of $\tilde{D}$ differs significantly between 850 and 200 hPa, the net stretching effect ($S1+S2$) becomes nearly equal (regardless of the sign) at both levels. Accordingly, the strong regulation of the sheared mean monsoon flow upon generation of 45-day vorticity perturbations is implied. At 200 hPa, the term A is positive because of a westward as well as an equatorward advection of anticyclonic $\tilde{\zeta}_{200}$ due to the prevailing summer mean northeasterly monsoon flow. In other words, the summer mean upper monsoon flow is responsible for removing anticyclonic $\tilde{\zeta}_{200}$ vorticity away from the convective forcing. The term B contributes to a further reduction of the anticyclonic $\tilde{\zeta}_{200}$ vorticity through an equatorward advection of $\langle\eta\rangle$ by a convectively induced anomalous Hadley circulation (Fig. 8c). As such, an important rôle of A and B is to inhibit an excess growth of the upper-tropospheric anticyclonic MJO immediately above

the convective center. In addition, $S2$ and N also act as opposing effects against the anticyclonic vorticity forcing by $S1$. Thus, at 200 hPa, the net anticyclonic forcing due to the sum of A, B, $S1$, $S2$ and N reduces to -1.3×10^{-11} s^{-2}, which is only about one third of $S1$.

Conversely, at 850 hPa, the $S1$ forcing effectively produces cyclonic vorticity, since the remaining effects of A, B, $S2$ and N almost canceled each other out. Namely, the net cyclonic forcing due to the sum of A, B, $S1$, $S2$ and N is approximately equal to $S1$ itself, amounting to 2.3×10^{-11} s^{-2}, which is nearly twice as large (sign omitted) as the corresponding net anticyclonic forcing at 200 hPa. The barotropic MJO-transient eddy interaction N appears to be insignificant over the monsoon domain. This is due to the fact that short-period transient disturbances are nearly isotropic, and do not cause any significant flux divergence of $\widetilde{\zeta' \boldsymbol{v}'}$.

Yet another important indication in Table 2 is that the average of $\tilde{\zeta}_{850}$ and $\tilde{\zeta}_{200}$ is not zero, but distinctly positive, and amounts to about 0.8×10^{-6} s^{-1} (cyclonic). Of course, a barotropic component such as the vertical mean cyclonic vorticity emerges as a result of the interaction of MJO with the horizontally, as well as vertically, sheared mean monsoon flow, as described earlier. If no shear is present in the mean monsoon flow, the response to convection is exactly out of phase (baroclinic) in the vertical. As will be shown later in Section 6, it is the convection-induced barotropic cyclonic vorticity that acts as an origin of the barotropic Rossby wave dispersion.

4. Northward phase propagation of MJO

The most notable feature of tropical MJO is its systematic northward progression across the confluence zone. Associated with this is the change in vertical structure of MJO from baroclinic in the Tropics (C_1 in Fig. 9c) to barotropic in the extratropics (for example, C_2 and A_2 in the same diagram). It is, therefore, required to further detail the nature of northward-propagating tropical MJO in order to fully understand its exact linkage with the mid-latitude ISO.

There exists a significant regional difference in the northward propagation of tropical MJO. Figure 10 presents category-latitude sections of $\tilde{T}_{BB}$ along four selected longitudes. The longitudes 80°–100°E are located in the midst of SEAM with strong climatological north-south heat contrasts between the cool Indian Ocean and the heated Asiatic Continent (including the Himalayan Massif). Weak $\tilde{T}_{BB}$ does exhibit an ill organized, intermittent northward propagation from the equator to about 20°–25°N, in qualitative agreement with the previous findings by Yasunari (1980) and Sikka and Gadgil (1980). The 45-day $\tilde{T}_{BB}$ variability becomes far more pronounced as one approaches the low-level monsoon confluence zone. At 110°–130°E (Fig. 10b), the northward propagation of $\tilde{T}_{BB}$ with a phase speed of 0.9 ms^{-1} is most clearly defined and causes an alternation between the distinct active monsoon with $\tilde{T}_{BB}$ as low as -7 K at Category 3 and the break monsoon with $\tilde{T}_{BB}$ as high as 7 K at Category 7, over the central Philippines (15°N, 110°–130°E). Holland (1995) postulated that the low-level confluence zone facilitates development of transient disturbances (including typhoons), eventually emanating trapped wave energy northward via the mean southerly steering current. It appears that Holland's postulation is valid for 45-day perturbations as well. As suggested in Fig. 9c, the active monsoon over and around the Philippines may act as the major energy source not only for the tropical MJO but also the mid-latitude ISO.

The longitudes 140°–160°E, which lie on the eastern end of the confluence zone, are also characterized by a systematic northward propagation of $\tilde{T}_{BB}$ from the equator to about 30°N (Fig. 10c). Here, the most active monsoon occurs at Category 4, *i.e.*, one category after the active monsoon at 110°–130°E. At Categories 3 and 4 (Figs. 7c and 7d), the low-level anomalous southeasterlies are responsible for furnishing moisture to the northern part of the convectively induced cyclonic circulation. This favors further northward progression of the tropical MJO-related convective system. When the tropical MJO encounters the climatological jet stream near 30°N, it rapidly dissipates and loses its identity due to an insufficient supply of moisture.

The manner in which moisture plays a vital rôle in the northward-propagating MJO system can be further elaborated by applying the 45-day filtering to each term in the moisture equation (not shown). The horizontal advection terms in the form of $\langle v \rangle \partial \tilde{q}/\partial y$ and $\tilde{v} \partial \langle q \rangle / \partial y$ are important in increasing $\tilde{q}$ poleward of the cyclonic center at an approximate rate of 1 and 3×10^{-5} g kg^{-1}s^{-1}, respectively, which facilitates moist $\tilde{q}$ perturbations to further shift northward. The total of these horizontal advection terms is about 19 g kg^{-1} per category (5.6 days), which is comparable to the climatological mean mixing ratio over the warm-pool region in the western Pacific. In comparison, the vertical advection terms, such as $\langle \omega \rangle \partial \tilde{q}/\partial p$ and $\tilde{\omega} \partial \langle q \rangle / \partial p$, do not contribute much to the northward phase propagation. This can be explained as follows: First, the climatological updraft $\langle \omega \rangle$ is strongest around 10°–15°N over the western North Pacific monsoon domain (Murakami and Matsumoto, 1994). $\tilde{\omega}$ is upward and strongest somewhere between 10° and 15°N (refer to minimal $\tilde{T}_{BB}$ and $\tilde{D}_{850}$ in Figs. 13a and 13b). Hence, both $\langle \omega \rangle \partial \tilde{q}/\partial p$ and $\tilde{\omega} \partial \langle q \rangle / \partial p$ tend to increase $\tilde{q}$ several degrees of latitude equatorward (not poleward) of the $\tilde{q}$ maximum located at 17°N (Fig. 13a). In other words, neither of the ver-

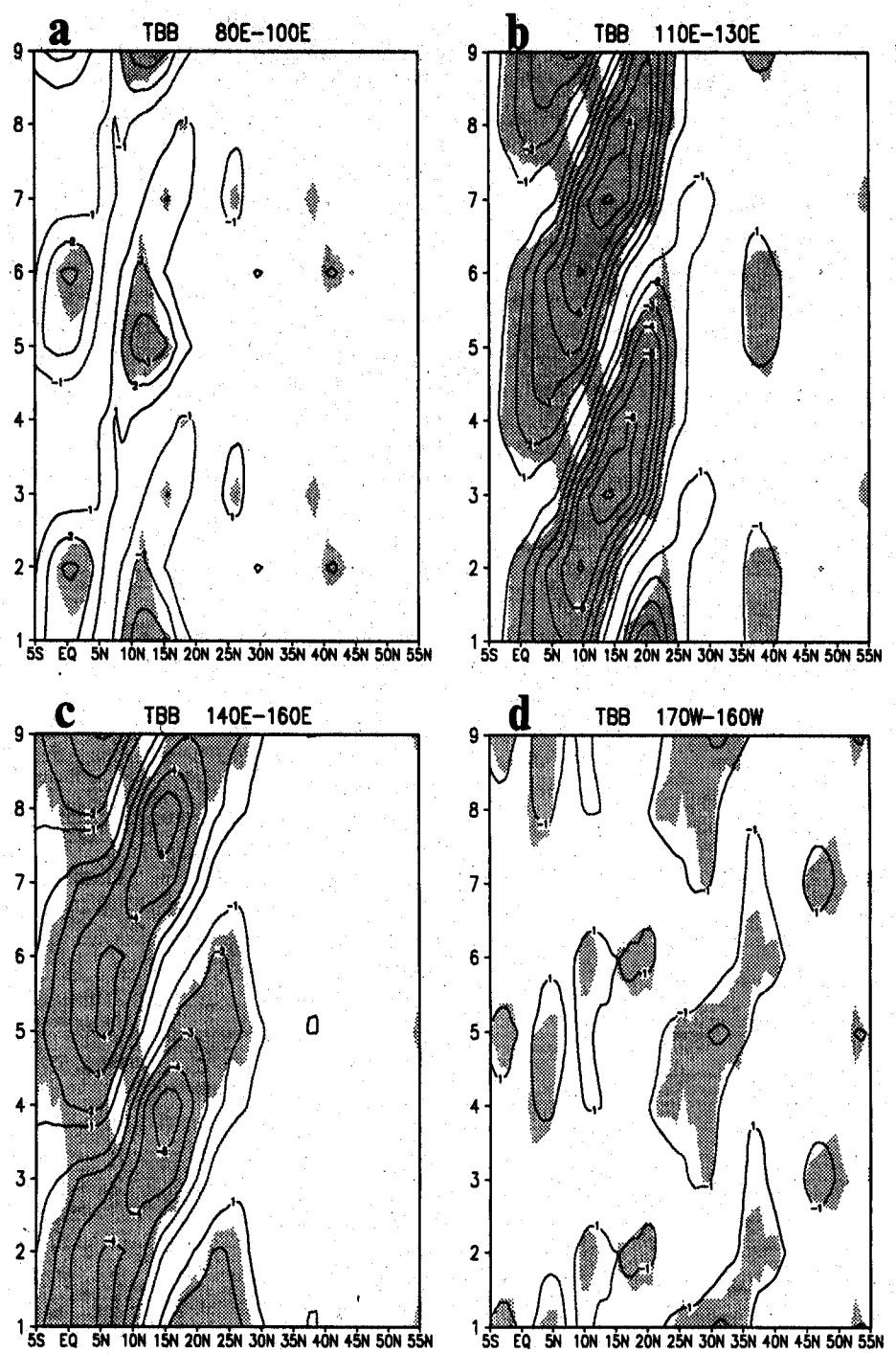

Fig. 10. Category-latitude sections of $\tilde{T}_{BB}$ (the interval is 1 K; no zero line) along 80°–100°E (a), 110°–130°E (b), 140°–160°E (c), and 170°–160°W (d), respectively. Shading is for regions surpassing the 95 % significant test.

tical advection terms makes a contribution to the northward migration of the MJO system. In this study, the use of only two levels of data at 850 hPa and 200 hPa inhibits an exact calculation of the moisture balance in the MJO system. A higher degree of vertical resolution is certainly desirable to remedy this deficiency.

In Fig. 10, the longitudes 170°–160°W traverse the climatological trade winds prevailing to the south of the Pacific High (see Fig. 2a). Here, the climatological summer mean $\langle q \rangle_{850}$ is lower than 8 g kg^{-1} poleward of the ITCZ. This results in somewhat weak $\tilde{T}_{BB}$ perturbations which intermittently migrate northward (Fig. 10d).

Figures 11a and 11b depict similarities as well as differences in the northward-propagating $\tilde{\zeta}_{850}$ and

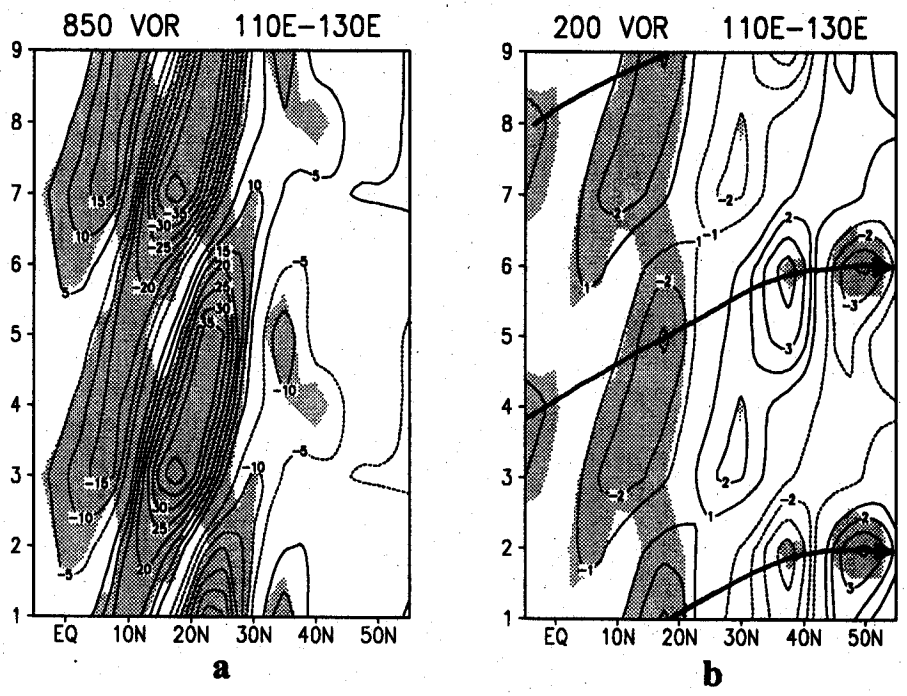

Fig. 11. Category-latitude sections of $\tilde{\zeta}_{850}$ (a; the interval is 5×10^{-7} s^{-1}) and $\tilde{\zeta}_{200}$ (b; the interval is 1×10^{-6} s^{-1}) along 110°–130°E. Heavy full arrows denote the group velocity phenomena as detailed in the text.

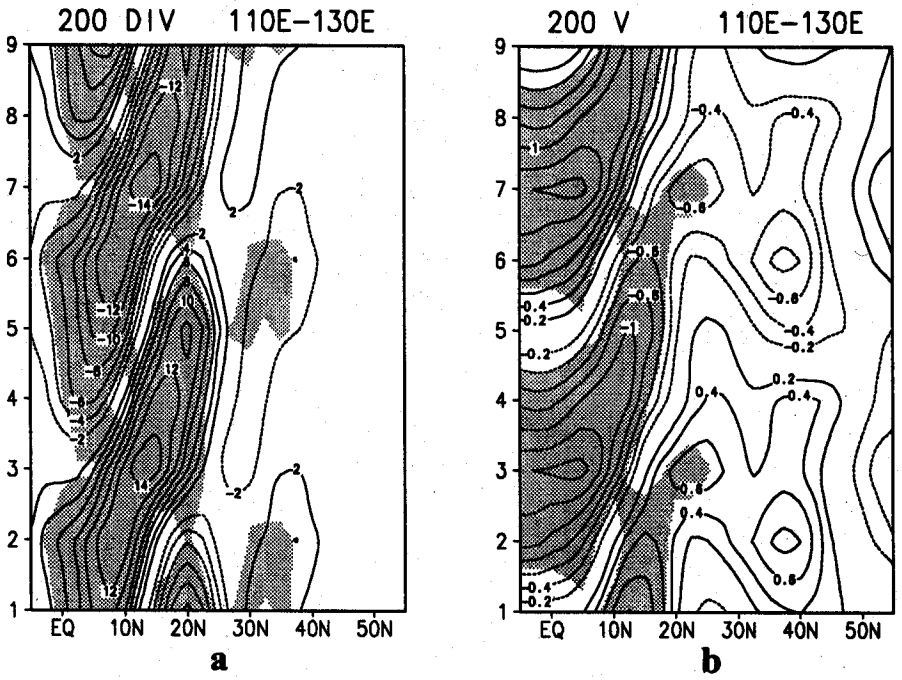

Fig. 12. As in Fig. 11, except for $\tilde{D}_{200}$ (a; the interval is 2×10^{-7} s^{-1}) and $\tilde{\nu}_{200}$ (b; the interval is 0.2 ms^{-1}) with no zero line.

$\tilde{\zeta}_{200}$ along 110°–130°E. Between the equator and about 25°N, $\tilde{\zeta}_{850}$ is nearly in parallel with $\tilde{\zeta}_{200}$, both exhibiting a similar northward propagation to that of $\tilde{T}_{BB}$ in Fig. 10b. When approaching the western Pacific subtropical ridge line near 25°N, both $\tilde{\zeta}_{850}$ and $\tilde{T}_{BB}$ suddenly collapse. Simultaneously, $\tilde{D}_{200}$ also collapses abruptly (refer to Fig. 12a). Poleward of 30°N, the convective activity becomes minimal (if any) and no significant variability of $\tilde{T}_{BB}$, $\tilde{\zeta}_{850}$ and $\tilde{D}_{200}$ is observed. Yet, $\tilde{\zeta}_{200}$ is still pronounced

and keeps moving persistently northward. How is it possible for non-divergent $\tilde{\zeta}_{200}$ perturbations to keep moving northward? Recall that MJO is made up of a wide range of periodicities from about 30 to 90 days. It is highly probable that MJO is dispersive and the energy of a wave group is concentrated in limited regions along its northward journey. In Fig. 11b, note a sudden amplification of a cyclonic cell near 37°N slightly prior to Category 6, followed by a similar sudden intensification of an anticylonic cell near 50°N by Category 6. If we consider the group velocity, it may be easy to understand these features. As illustrated by heavy arrows in Fig. 11b, the suggested group velocity is about 5 ms^{-1}, which is almost 10 times faster than the northward phase speed of individual carrier waves. This energy propagation is also evident from the wave train along a great circle traversing the North Pacific (Fig. 9c).

The category-latitude section of $\tilde{u}_{200}$ along 110°–130°E is not reproduced here, since $\tilde{u}_{200}$ largely represents the rotational part of the winds so that the derivative $\partial\tilde{u}_{200}/\partial y$ is inversely proportional to $\tilde{\zeta}_{200}$. As in $\tilde{\zeta}_{200}$, $\tilde{u}_{200}$ perturbations also migrate northward all the way to 50°N with a distinct group velocity phenomenon (or amplitude modulation). As shown in Fig. 12b, on the other hand, $\tilde{v}_{200}$ perturbations behave differently without any indication of northward propagation poleward of 30°N. This is due to the fact that $\tilde{v}_{200}$ represents primarily the divergent part of the winds in the Tropics, whereas it is dominated by the rotational part of the winds poleward of 30°N. In the Tropics, $\tilde{v}_{200}$ is basically induced by convection and its derivative $\partial\tilde{v}_{200}/\partial y$ is approximately proportional to $\tilde{D}_{200}$ (compare Figs. 12a and 12b). In the mid-latitudes, $\tilde{v}_{200}$ is no longer divergent, but rotates around the vorticity center. As an example, the southerly $\tilde{v}_{200}$ near 37°N at Category 2 (Fig. 12b) represents the anticyclonic flow along the western periphery of an anticyclonic cell (Fig. 8b).

Before closing this section, a brief comment is given pertaining to the vertical structure of the tropical MJO by showing Fig. 13, which is for 110°–130°E at Category 3. Similar diagrams of the same format for different longitudes and categories are not reproduced here to save space. At Category 3, convection is strongest at 14°N with a minimum $\tilde{T}_{BB}$ there. At the same latitude, a minimum $\tilde{D}_{850}$ coincides with a zero $\tilde{v}_{850}$, while a maximum $\tilde{D}_{200}$ also agrees with a zero $\tilde{v}_{200}$, indicating that $\tilde{v}$ is divergent. There exists an inverse correlation between $\tilde{v}_{850}$ and $\tilde{v}_{200}$, implying an anomalous local Hadley circulation. This Hadley circulation is asymmetric with respect to the convective center, as manifested by stronger equatorward outflow as against much weaker poleward outflow at 200 hPa. At the equator, the product of $\tilde{v}_{200}$ by $\tilde{u}_{200}$ is positive, *i.e.*, an export of easterly momentum into the Southern Hemisphere upper troposphere. In fact, $\tilde{u}_{200}\tilde{v}_{200}$ is positive without regard to category, thus contributing to a weakening of the climatological summer mean easterlies over the WNPM domain at 200 hPa. A similar argument also applies to the product of $\tilde{v}_{200}$ by $\tilde{T}_{200}$, which is negative throughout one cycle of MJO and indicates a cross-equatorial export of sensible heat, thus reducing the mean potential energy generated by the climatological north-south heat contrasts.

Of particular interest in Fig. 13 is the occurrence of largest $\tilde{q}_{850}$, as well as highest $\tilde{T}_{200}$, about 3 degrees of latitude northward of the convective center. The moist static energy, as defined by $c_p\tilde{T}+\tilde{\phi}+L\tilde{q}$, is estimated to be 855 m^2s^{-2} at 850 hPa and 242 m^2s^{-2} at 200 hPa. The moist unstable vertical stratification ahead of convection certainly facilitates the further northward progression of tropical MJO across the tropical ocean. No large land mass is present eastward of about 130°. Yet, the tropical MJO exhibits a distinct northward migration over the western North Pacific. Apparently, theories based on the land surface hydrological cycle cannot explain the northward propagation over the western Pacific.

5. Mean flow-MJO/ISO interaction

The previous statement that the tropical MJO is of convective origin, while the mid-latitude ISO is basically of non-divergent (barotropic) character requires further elaboration. In general, the kinetic energy equation is utilized when investigating the mechanisms through which disturbances grow. However, we find it more useful to introduce the enstrophy equation from Eq. (1) since it includes divergent terms $S1$ and $S2$ which explicitly reflect the convective forcing of vorticity. To this end, we multiply both sides of Eq. (1) by $\tilde{\zeta}$ and integrate by parts over an extensive domain S. The resulting equation can be expressed as

$$\frac{\partial Z_i}{\partial t} = CZ_i + CI_i + CF_i + CB_i, \tag{2}$$

where

$$Z_i = \frac{1}{S}\int\int_S \frac{1}{2}\tilde{\zeta}_i^2 dS, \tag{3}$$

$$CZ_i = -\frac{1}{S}\int\int_S \tilde{\boldsymbol{v}}_i\tilde{\zeta}_i\cdot\nabla\langle\eta\rangle\, dS, \tag{4}$$

$$CI_i = -\frac{1}{S}\int\int_S \left\{\langle\eta\rangle\,\tilde{\zeta}_i\tilde{D}_i + \frac{1}{2}\langle D\rangle\,\tilde{\zeta}_i^2\right\} dS, \tag{5}$$

$$CF_i = -\frac{1}{S}\int\int_S \tilde{\zeta}_i\nabla\cdot(\widetilde{\zeta'\boldsymbol{v}'})_i dS, \tag{6}$$

$$CB_i = -\oint_l \frac{\tilde{\zeta}_i^2}{2}\langle\boldsymbol{v}\rangle\,\hat{n}dl, \tag{7}$$

in which the suffix i refers to the quantities at category i. A positive sign of CZ_i indicates an intensification of the enstrophy Z_i when the vorticity flux

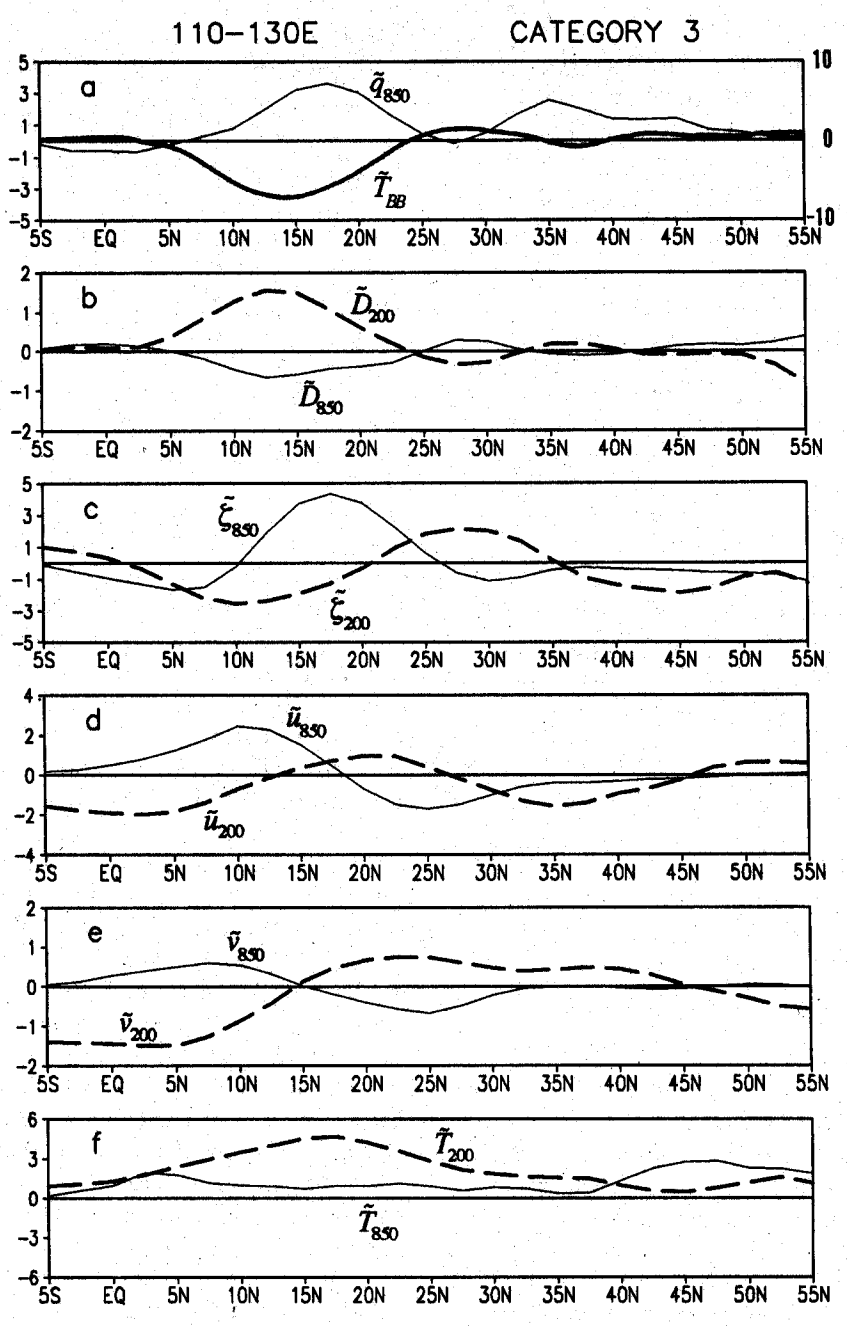

Fig. 13. Latitudinal profiles of (a) $\tilde{T}_{BB}$ (the units are K; see the right-hand side of the vertical axis) and $\tilde{q}_{850}$ (the units are 10^{-1} g kg^{-1}), (b) $\tilde{D}_{850}$ and $\tilde{D}_{200}$ (the units are 10^{-6} s^{-1}), (c) $\tilde{\zeta}_{850}$ and $\tilde{\zeta}_{200}$ (the units are 10^{-6} s^{-1}), (d) $\tilde{u}_{850}$ and $\tilde{u}_{200}$ (the units are ms^{-1}), (e) $\tilde{v}_{850}$ and $\tilde{v}_{200}$ (the units are ms^{-1}), and (f) $\tilde{T}_{850}$ and $\tilde{T}_{200}$ (the units are 10^{-1} K), averaged between 110°–130°E at Category 3.

$\tilde{v}_i\tilde{\zeta}_i$ is directed down the gradient of the climatological summer mean absolute vorticity. A positive sign of CI_i is defined for a baroclinic growth of the enstrophy Z_i, while CF_i signifies a non-linear barotropic interaction between MJO and transient eddies (< 15 days), and contributes to intensify Z_i when cyclonic (anticyclonic) $\tilde{\zeta}_i$ coincides with the vorticity flux convergence (divergence) due to eddies. Finally, CB_i is defined as the boundary flux term that represents an export or import of $\tilde{\zeta}_i^2$.

Table 3A presents computed results of Z_i, CZ_i, CI_i, CF_i and CB_i at each category, averaged over the Region A (see Fig. 9) covering both SEAM and WNPM. A positive CI_i indicates a convective forcing of Z_i, which is nearly equal at both 200 and 850 hPa. At 850 hPa, the convective forcing is further reinforced by the positive CZ_i process, while CI_i is largely compensated for by the negative CZ_i at 200 hPa. This is consistent with a larger enstrophy Z_i at 850 hPa than at 200 hPa (Table 3A). Here, emphasis is placed on the fact that the dynamical

Table 3A. Mean values of Z (10^{-13} s^{-2}), and CZ, CI, CF and CB (10^{-18} s^{-3}), averaged over the region A at each category.

A (0°–30°N, 60°–150°E)				
Category	1	2	3	4
Z_{200}	8.1	4.5	8.7	8.8
CZ_{200}	−6.0	−2.1	−5.5	−8.9
CI_{200}	11.5	2.6	13.2	14.3
CF_{200}	−0.1	−0.4	−1.6	−0.7
CB_{200}	−0.2	−0.8	0.1	0.5
Z_{850}	9.1	6.2	14.1	11.3
CZ_{850}	3.6	1.9	5.7	5.0
CI_{850}	10.3	6.4	14.3	12.9
CF_{850}	−1.2	−0.9	−1.5	−0.9
CB_{850}	0.1	0.0	0.1	0.1

Table 3B. As in Table 3A, except for the region B.

B (30°–60°N, 150°E–140°W)				
Category	1.	2	3	4
Z_{200}	31.7	14.9	39.2	16.5
CZ_{200}	1.2	6.8	11.0	−0.6
CI_{200}	−1.3	−6.1	−13.1	0.5
CF_{200}	−0.5	3.2	5.8	−1.6
CB_{200}	−1.9	−3.3	−11.7	−1.3
Z_{850}	5.4	4.1	9.3	3.8
CZ_{850}	0.4	0.2	0.9	0.0
CI_{850}	2.0	1.5	3.4	0.8
CF_{850}	−0.1	−0.2	0.3	0.0
CB_{850}	−0.6	0.2	−0.1	0.3

structure of MJO in the vertical is determined not only by the convective forcing CI_i, but also by the MJO—mean monsoon flow interaction, as denoted by CZ_i. At 200 hPa, there exists a somewhat strong equatorward flux of anticyclonic vorticity ($\tilde{v}_i\tilde{\zeta}_i > 0$) in the direction of decreasing climatological planetary vorticity (see Figs. 8c and 9a), resulting in negative CZ_i, *i.e.*, MJO furnishing enstrophy to the mean monsoon flow. At this level, the vorticity flux $\tilde{v}_i\tilde{\zeta}_i$ is largely accomplished by the divergent part of the winds as manifested by the exceptionally strong equatorward upper-tropospheric Hadley circulation. At 850 hPa, on the other hand, $\tilde{v}_i\tilde{\zeta}_i$ sensitively depends on the rotational part of the winds. An inspection of Fig. 7c, together with Fig. 9c, reveals an equatorward flux of cyclonic vorticity against the gradient of the mean absolute vorticity $\langle\eta\rangle$, *i.e.*, an increase in eddy Z_i (positive CZ_i) at the expense of enstrophy in the mean flow. The non-linear interaction term CF_i is negative, although small, at both 850 and 200 hPa, reflecting a tendency for MJO to enhance short-period transient eddies. CB_i is also small over the monsoon domain.

To monitor the enstrophy budget of the midlatitude ISO, we have chosen the Region B extending

Table 3C. As in Table 3A, except for the region C.

C (35°–55°N, 180°–140°W)				
Category	1	2	3	4
Z_{200}	34.0	14.7	55.8	17.7
CZ_{200}	15.2	8.3	21.2	−1.3
CI_{200}	−1.4	2.0	−29.1	−8.6
CF_{200}	−8.8	2.2	13.7	3.2
CB_{200}	−1.9	−12.4	−1.1	7.2
Z_{850}	4.1	3.5	14.4	5.4
CZ_{850}	0.6	0.3	1.6	−0.2
CI_{850}	−0.1	1.1	4.2	0.3
CF_{850}	0.5	0.5	0.2	0.6
CB_{850}	−0.9	−0.5	0.7	−0.1

from 30° to 60°N and between 150°E and 140°W, covering the major portion of the jet stream. Here, the salient features noted at 200 hPa in Category 3 are as follows: (1) CZ_i is the major contributor to intensification of Z_i, (2) CI_i has a tendency to damp Z_i, (3) CF_i is as important as CZ_i, both contributing to barotropic amplification of Z_i , and (4) a negative CB_i implies an export of enstrophy across the eastern (140°W) boundary toward the North American Continent, as well as through the southern (30°N) boundary into the TUTT region. In other words, the North Pacific upper tropospheric jet is responsible for generation of a large amount of enstrophy via CZ_i and CF_i, and for supporting the mid-latitude ISO activities elsewhere. At 850 hPa, on the other hand, an approximately isotropic structure of the low-level, mid-latitude ISO (see Fig. 7c, for example) relegates the rôle of CZ_i and CF_i to that of secondary importance. At this level, CI_i appears to be the effective contributor to Z_i.

Next, we have deliberately selected a small region C to specifically monitor the strong activity of $\tilde{\zeta}_{850}$ and $\tilde{\zeta}_{200}$ in the immediate vicinity of the jet exit at Category 3 (refer to Figs. 9a and 9c). In Category 3, both CZ_i and CF_i at 200 hPa become much more pronounced than those averaged over the entire jet stream region shown in Table 3B. At 850 hPa, CI_i is relatively important compared to CZ_i, while CF_i changes to a minor term. Here, caution must be exercised when interpreting the physical meaning of each term in Eq. (2) at the respective levels of 850 hPa and 200 hPa. Strictly speaking, Eq. (2) is valid only after vertically integrating it throughout the atmosphere. In the present study, the vertical integration is approximated by the sum of each term at the two levels of 850 hPa and 200 hPa. Over the Region C, the vertical sums at Category 3 are as follows: $CZ_i = 22.8$, $CI_i = -24.9$, $CF_i = 13.9$, and $CB_i = -0.4$. This summarizes the enstrophy budget at the jet exit region. Namely, (1) the barotropic mean flow—ISO interactions, as well as the non-linear barotropic interactions of ISO with

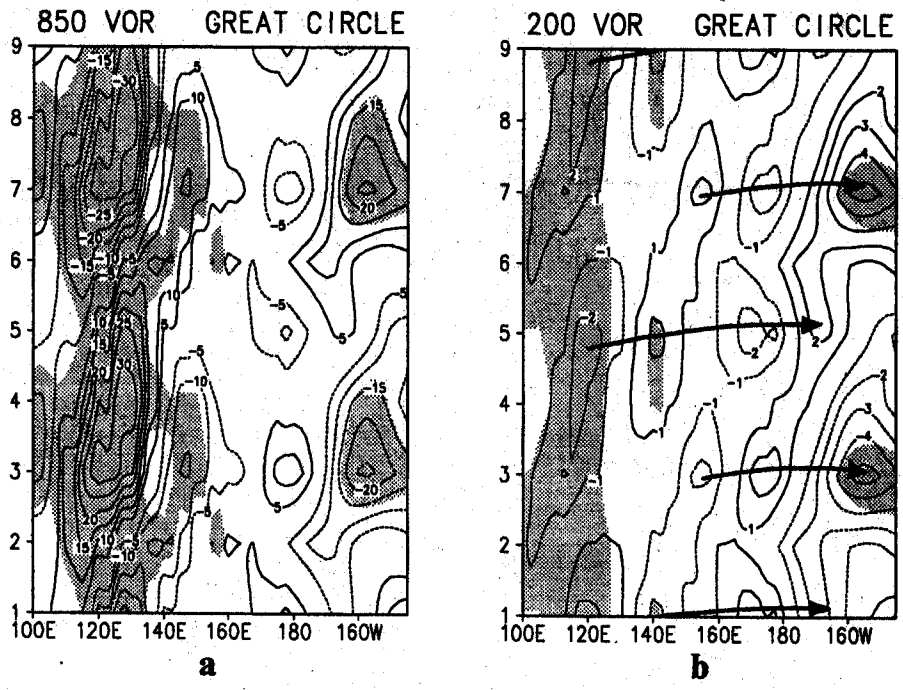

Fig. 14. Category-longitude distribution of $\tilde{\zeta}_{850}$ (a; the interval is 5×10^{-7} s^{-1}) and $\tilde{\zeta}_{200}$ (b; the interval is 1×10^{-6} s^{-1}) with no zero line along the great circle identified in Fig. 9c. Heavy full arrows indicate the group velocity phenomena as detailed in the text.

short-period disturbances, are primarily responsible for amplification of ISO, and (2) mid-latitude ISO does not owe its existence to the baroclinic CI_i process.

6. Rossby-wave dispersion

Evidence has been presented that the southwestern end of the North Pacific is characterized by prominence of convectively forced tropical MJO, while the northeastern corner represents the region of most pronounced barotropic mid-latitude ISO. Interestingly, these two locations nearly coincide with those of preferred forcing and strongest response occurring in a barotropic model (Simmons *et al.*, 1983) with the initial state prescribed by the climatological streamfunction at 300 hPa, which was then perturbed by adding a localized forcing (see Fig. 5 of their paper). A different view was proposed by Hoskins and Karoly (1981) who interpreted a wave train emanating out of a localized forcing as the refraction of two-dimensional dispersive Rossby waves in the sheared mean basic flow.

The present observational study also confirmed the occurrence of a wave train of cyclonic and anticyclonic cells approximately aligned along a great circle that intersects the convective center near the Philippines (see Fig. 9c). We have projected the profile of $\tilde{\zeta}_{850}$ and $\tilde{\zeta}_{200}$ along the great circle on to the x-axis in each category, as shown in Figs. 14a and 14b, respectively. At 850 hPa, $\tilde{\zeta}_{850}$ propagate eastward from 100° to 160°E, this also indicating the northward migration of $\tilde{\zeta}_{850}$ across the confluence zone. Beyond 160°E, the phase propagation of $\tilde{\zeta}_{850}$ becomes irregular. At 200 hPa, $\tilde{\zeta}_{200}$ exhibits a systematic eastward propagation all the way from 100°E to about 150°W with an average speed of 1.3 ms^{-1}. Also evident is an amplitude modulation of $\tilde{\zeta}_{200}$ perturbations, as illustrated by heavy arrows. For example, a sequence of events occurring around Category 5 is as follows: The anticyclonic cell first amplifies near 120°E slightly prior to Category 5, followed by a downstream intensification of the cyclonic cell near 140°E. Further eastward, another anticyclonic cell develops near 170°E slightly after Category 5. In the same manner, development of a strong anticyclonic cell near 150°W (the northeastern North Pacific) occurs nearly simultaneously with an upstream amplification of a similar anticyclonic cell near 150°E at Category 3, which corresponds to the time of most active convection over the southwestern North Pacific (*i.e.*, near the Philippines). As such, Fig. 14b is a simple realization of the Rossby-wave dispersion, although it is not as clearly defined as one would like. Similar Rossby-wave dispersion, although not as distinct as that at 200 hPa, can also be detected in Fig. 14a for 850 hPa.

An effort has so far been made to detail the vertical dependence of $\tilde{\zeta}$ by utilizing only two levels of data at 850 and 200 hPa, at which levels satellite-

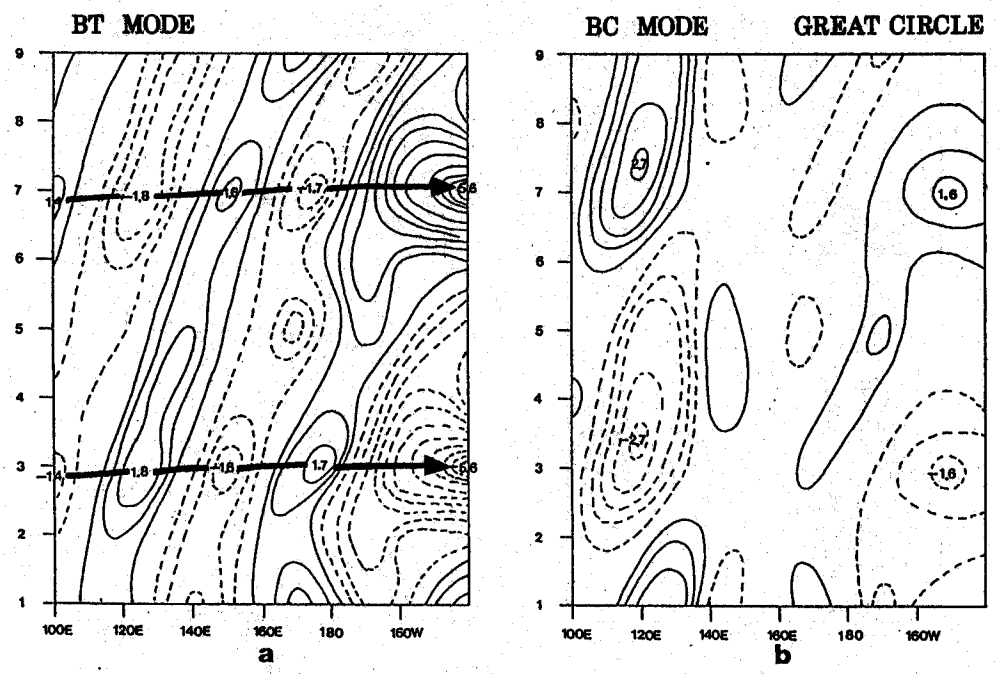

Fig. 15. As in Fig. 14, but for $\tilde{\zeta}_{BT}$ (a; the interval is 0.5×10^{-6} s^{-1}) and $\tilde{\zeta}_{BC}$ (b; the interval is 0.5×10^{-6} s^{-1}). Refer to Eq. (8) for definition of $\tilde{\zeta}_{BT}$ and $\tilde{\zeta}_{BC}$.

observed winds are available. Within the scope of the present study, the two-layer representation appears to be adequate. However, a more effective way of describing the barotropic Rossby-wave dispersion requires partitioning of $\tilde{\zeta}$ into two components as follows:

$$\tilde{\zeta}_{BT} = (\tilde{\zeta}_{200} + \tilde{\zeta}_{850})/2, \ \tilde{\zeta}_{BC} = (\tilde{\zeta}_{200} - \tilde{\zeta}_{850})/2, \quad (8)$$

where the first component (signified as $\tilde{\zeta}_{BT}$) represents a barotropic mode defined by averaging $\tilde{\zeta}_{850}$ and $\tilde{\zeta}_{200}$, while the second component (marked as $\tilde{\zeta}_{BC}$) corresponds to a baroclinic mode defined by the difference between $\tilde{\zeta}_{850}$ and $\tilde{\zeta}_{200}$. In Figs. 15a and 15b are plotted the profiles of $\tilde{\zeta}_{BT}$ and $\tilde{\zeta}_{BC}$ along the great circle.

The most notable feature in Fig. 15a is a quite regular northeastward propagation of $\tilde{\zeta}_{BT}$ perturbations, which are oriented in the convective monsoon domain around 5°N, 100°E and terminating at the jet exit region near 50°N, 160°W. As emphasized earlier, the tropical barotropic (BT) mode emerges when a convectively induced MJO interacts with the horizontally as well as vertically sheared mean monsoon flow. Figure 15a also indicates two occasions of well organized amplitude modulation of barotropic $\tilde{\zeta}_{BT}$ perturbations (heavy arrows). At Category 3, for example, a distinct wave train of three anticyclonic cells at 100°E, 150°E and 140°W, is alternated by two cyclonic cells near 120°E and 170°E, respectively, along the great circle. Of interest is that this wave train of $\tilde{\zeta}_{BT}$ is much more clearly defined than those for individual vorticity perturbations of $\tilde{\zeta}_{850}$ (Fig. 14a) and $\tilde{\zeta}_{200}$ (Fig. 14b). Namely, it is the barotropic mode $\tilde{\zeta}_{BT}$ that is primarily responsible for transporting energy northward via the Rossby-wave dispersion processes.

Next, let us turn our attention to Fig. 15b for the baroclinic (BC) mode. One may note an intermittent and somewhat irregular phase propagation of $\tilde{\zeta}_{BC}$ perturbations. Associated with this is an absence of any noticeable Rossby-wave dispersion of baroclinic carrier waves. In short, the BC mode contributes little to the tropical-extratropical interaction. As such, mid-latitude BC perturbations can develop without any apparent influence of tropical BC disturbances. One example is an amplification of a mid-latitude anomalous anticyclonic cell near 150°W at Category 3, that occurs several days prior to (not after) the maximum intensification of a tropical anomalous anticyclone around 120°E (Fig. 15b). Most probably, the two anticyclonic cells under consideration are independent of each other. Furthermore, the two anomalous anticyclones are of completely different origin. The tropical BC owes its origin to convection and, thus, the mean monsoon flow does not exert any dominant rôle upon the BC development. Conversely, the presence of vertical shear in the mean jet stream is absolutely necessary for the development of mid-latitude BC perturbations. We refer to the Kawamura and Murakami's (1995) observation that mid-latitude ISO is partially enhanced by the baroclinic instability of the mean jet stream since ISO tends to reduce vertical shear of the jet by transporting sensible heat northward.

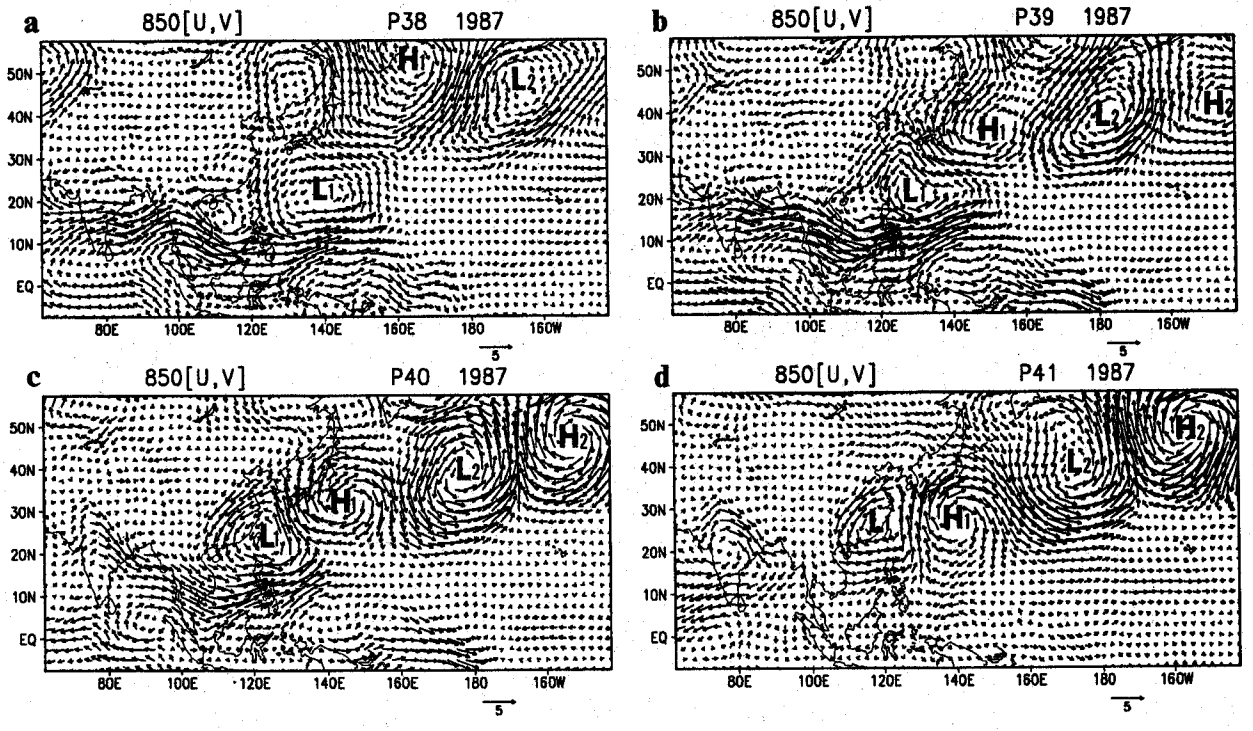

Fig. 16. Pentad mean ($\tilde{u}_{850}$, $\tilde{v}_{850}$) winds (reference arrow 5 ms^{-1}) from Pentad 38 (a) to Pentad 41 (d) during the 1987 summer. Major cyclonic and anticyclonic disturbances are marked by L_i and H_i ($i = 1,2$).

At any rate, the most important implication in Fig. 15b is that the BC mode is not capable of producing any significant tropical-extratropical interaction on the 45-day time scale.

Before closing this section, let us once again take a look at Fig. 9c, which reveals that the wave train is realized only in the Category 3 composite map of 850-hPa winds. Recall that the Category-3 pattern was defined by averaging 26 pentad-mean wind fields selected with reference to changes in $\tilde{T}_{BB}$ within the confluence zone. An inspection of these 26 individual maps does indicate several occasions of the Rossby-wave dispersion. An example is shown in Fig. 16, which presents a series of pentad-mean 850-hPa winds from Pentad 38 (July 5–9) to 41 (July 20–24) during the 1987 summer. At Pentad 38, a cyclonic cell (signified as L_1) begins to intensify near the eastern periphery of an anomalous monsoon trough. The L_1 becomes fully established by Pentad 39, when the anomalous westerlies to its south also intensify. The convection-induced L_1 moves northwestward between Pentad 39 and 41, which shows an example of the northward migration of MJO. The westerlies over India and the Bay of Bengal considerably weaken after Pentad 40. These features are perhaps a manifestation of an eastward wave energy propagation between Pentad 38 and 40. The intensification of L_1 occurs as a part of this eastward wave energy propagation. By Pentad 40, the wave train structure becomes clearly defined, diagonally crossing the North Pacific. It is not until Pentad 41 when the anticyclonic cell H_2 becomes most intensified near the northeastern corner of the North Pacific. From an inspection of all of 26 cases, we find recurrence of similar Rossby-wave dispersion patterns with an approximate time scale of 45 days over the North Pacific. Thus, the Rossby-wave dispersion is not fortuitous but a statistically reliable event.

7. Discussion and concluding remarks

Some of the major results obtained in the present study are schematically summarized in Fig. 17. The 45-day convective activities are most pronounced within the monsoon confluence zone (dark shading). In this region, tropical MJO is of convective origin as confirmed from an evaluation of CI in Eq. (2). The lower tropospheric cyclonic response (marked as C_1) is very pronounced due to the presence of the convergent and cyclonically sheared climatological low-level monsoon flow. To the south and west of C_1 are strong anomalous westerlies extending as far west as the western tropical Indian Ocean, which is considered as a Rossby-wave response.

Weak but significant anomalous easterlies are enhanced over the tropical central Pacific east of the active convection as a result of Kelvin-wave response. The low-level easterly anomalies are accompanied by upper-level westerly anomalies, forming a Walker circulation-like structure. The lower tropo-

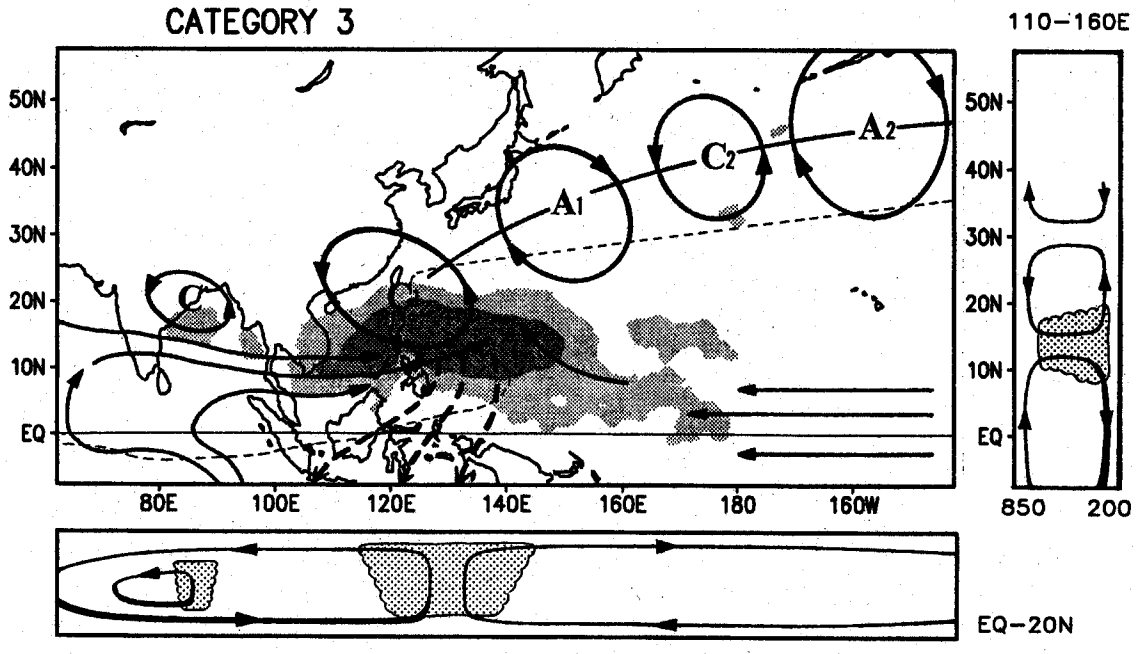

Fig. 17. Schematic diagram of 45-day filtered 850- and 200-hPa circulations, composited with reference to active convection (dark shading) near the Philippines. The low-level anomalous circulation induced by intense convection is denoted by solid lines, whereas heavy dashed lines indicate the upper-level outflow towards the equator. The lower tropospheric response (signified as C_1) and associated extratropical Rossby wave train (signified as A_1, C_2 and A_2) are observed. The thin dashed line denotes the border between the climatological low-level westerlies and easterlies. The bottom diagram emphasizes zonal asymmetry of anomalous local Walker circulation with strong low-level westerly anomalies. The right diagram shows the meridional asymmetry of anomalous local Hadley circulation characterized by dominant upper-level cross-equatorial outflow.

spheric response to convective heating is very similar to the steady response to heating away from the equator, demonstrated by Gill (1980). Here, the lower tropospheric response to the MJO convective system in the WNPM domain is characterized by a strong zonal asymmetry, such that the low-level western response is much stronger than the low-level eastern response, as indicated in the bottom diagram.

On the other hand, the upper tropospheric anticyclonic response to convective heating is much less pronounced due to the influence of the divergent and anticyclonically sheared upper-level monsoon flow. The most notable feature of the upper tropospheric response is the strong equatorward outflow indicated by thick dashed arrows, which is much stronger than the poleward counterpart, as we emphasized in the right-side diagram. An important rôle of the equatorward outflow is to export anticyclonic vorticity into the Southern Hemisphere upper troposphere, thus inhibiting an excessive growth of the MJO anticyclonic vorticity above the convective center. As shown in Fig. 17, the northward-propagating MJO prevailing over the western North Pacific, away from the equator, leads to strong horizontal and vertical asymmetries in the convection-induced circulation. We emphasize that such asymmetries are reinforced by the mean monsoon flow - MJO interaction.

The tropical MJO in the western Pacific region exhibits a systematic northward progression, through which it can excite and interact with the mid-latitude ISO. Simultaneously with the occurrence of most-active convection near the Philippines, there is a formation of a lower-tropospheric wave train extending to the mid-latitude (C_1–A_1–C_2–A_2) approximately along the great circle (Fig. 17). C_1 is, of course, forced by convection and hence, essentially baroclinic in the vertical. However, a substantial BT component is also included in C_1. This is substantiated by looking at Figs. 15a and 15b, which indicates that the ratio of the BT to BC component near 120°E (convective region) is about one to three or less (sign omitted). The reverse is true for A_1, C_2 and A_2. They are of approximately barotropic character, since BT is more than three times as large as BC (without regard to sign). It seems that the barotropic component of C_1 tends to excite a barotropic Rossby wave train of A_1, C_2 and A_2. This pattern is similar to what is commonly referred to as the Rossby wave dispersion emanating out of the actively convective region; in this case, the vicinity of the Philippines.

Previous numerous studies (*e.g.*, Sardeshmukh and Hoskins, 1988; Webster and Chang, 1988) on extratropical Rossby wave trains emanating out of convective heating have focused on the upper troposphere in winter hemisphere, because the climatological upper-level westerlies intrude equatorward to allow wave energy to propagate poleward. As a result, wave train-like features are most likely clearer in the upper troposphere. However, the situation is very different in the western Pacific region, where the summertime climatological low-level westerlies stretch all the way from the Philippines, via Japan, to as far northeast as the Aleutian Islands (Fig. 2a). Presumably, these westerlies act as a duct for the wave energy propagation to penetrate deep into the higher latitude region. Within the monsoon domain, the cyclonic shear embedded in the low-level monsoon westerlies favors establishment of a barotropic mode, as stated many times earlier. This also makes it easy for the emanation of barotropic wave energy from the moist (tropical) to dry (extratropical) region. So in that sense, the mean monsoon flow with a strong vertical shear seems to play a role in propagation of MJO-related wave energy into the extratropics, which is supported by Wang and Xie (1996).

An alternative view interprets the mid-latitude ISO as the most rapidly growing mode associated with a barotropic instability of the sheared local mean flow (Simmons *et al.*, 1983). Our enstrophy budget study indicates that in the extratropical upper troposphere barotropic instability makes a major contribution to the growth of the vorticity anomaly (such as A_2). This is especially evident near the Pacific jet exit region. It is likely that the *in-situ* barotropic instability is triggered by a Rossby-wave dispersion emanating out of a localized convection just east of the Philippines.

Evidence has been provided in this study that the northward propagation of tropical MJO is statistically significant and unique to the western North Pacific during the mid-summer of June to September, the months of a well established confluence zone sandwiched between the WNPM monsoon westerlies and the North Pacific trade wind easterlies. During May (pre-WNPM month), an ill organized confluence zone is located over the equatorial Bay of Bengal. As the season advances, the confluence zone extends eastward as well as northward, covering the entire WNPM domain from about 120° to 160°E between the equator and 30°N. The prominent climatological southerlies are embedded within the confluence zone (Fig. 2a). These climatological southerlies $\langle \nu \rangle$ carry $\tilde{q}$ moisture to as far north as Japan and possibly beyond, bring about negative $\langle \nu \rangle \, \partial \tilde{q} / \partial y$. On the other hand, convection which is asymmetric about the equator (Fig. 6c) induce a Rossby-wave response with the low-level anomalous cyclone displaced to the northwest of the convective center (Fig. 7c). This structural feature of MJO favors the transport of climatological mean moisture $\langle q \rangle$ poleward of the cyclonic center due to the prevailing southeasterlies $\tilde{\nu}$ (Fig. 7c), which results in negative $\tilde{\nu} \partial \langle q \rangle / \partial y$. The net effect of $\langle \nu \rangle \, \partial \tilde{q} / \partial y$ and $\tilde{\nu} \partial \langle q \rangle / \partial y$ is to contribute to the northward propagation of moist $\tilde{q}$ perturbations. Due to this reason, the confluence zone is characterized by a distinct northward phase propagation of tropical MJO. The confluence zone is also a region of the largest variability of MJO (Fig. 2c). The MJO activity and its associated northward phase propagation becomes less distinct as one approaches westward (eastward) to the India - Indochina (eastern Pacific) region. By October, the confluence zone retreats equatorward to the south of 15°–20°N, which is unfavorable for MJO to propagate northward. In short, the northward propagation is a regional-scale phenomenon and season dependent, predominating only during mid-summer. Associated with the northward propagation is the establishment of the statistically significant Rossby-wave dispersion emanating out of the convective forcing east of the Philippines. This stands in sharp contrast to what was found by Knutson and Weickmann (1987), that the extratropical response to tropical MJO is not statistically reliable. However, their study is subjected to some questions. First, their study was based on the six-month data from May (late spring) to October (mid-fall). Such a long record of data is not free from a chance that the entirely different, season dependent, MJO régimes are mixed up together, thus making it difficult to extract information only for summer. Second, in their study, reference was made to an eastward-propagating tropical MJO of relatively poor statistical reliability. As reported by Murakami (1987), the eastward progression of equatorial OLR in boreal summer occurs only about 54 % of the 5-year observing period of 1979–83. [In comparison, this study confirms the occurrence of northward migration of $\tilde{T}_{BB}$ across the confluence zone to be slightly more than 80 % of the total 9-year summers.] Third, their study was focused on the global-scale aspect of the extratropical response to tropical MJO. Are the global-scale summertime ISO perturbations with the time scales of about 45 days statistically reliable? The observational information has been too scanty to answer this question properly. Further study is required.

Acknowledgments

The first author is indebted to Dr. T.A. Schroeder for giving him an opportunity to engage in research at the University of Hawaii. We are grateful to Dr. J. Matsumoto and the anonymous reviewers for their helpful comments, which led to an improved presentation of the manuscript. This research was also partially supported by the JACCS program of the

Japan Science and Technology Agency. This is the School of Ocean and Earth Science and Technology publication 4148.

Appendix

List of Symbols

u, v	Zonal and meridional winds
ϕ	Geopotential height
T	Temperature
q	Mixing ratio of water vapor
f	The Coriolis parameter
ζ	Relative vorticity
D	Divergence
T_{BB}	Infrared equivalent black body temperature measured by Japanese geostationary satellites
Z	Enstrophy defined by Eq. (3)
CZ	Barotropic mean flow - MJO/ISO interaction defined by Eq. (4)
CI	Baroclinic forcing of MJO/ISO defined by Eq. (5)
CF	Non-linear interaction of MJO/ISO with short-period transient eddies defined by Eq. (6)
CB	Boundary flux defined by Eq. (7)
$\langle\ \rangle$	Climatological summer mean
$\tilde{(\ )}$	45-day transients
$(\ )'$	Transient eddies with periods shorter than about 15 days
SEAM	Summer monsoon over Southeast Asia (5°–20°N, 60°–100°E)
WNPM	Summer monsoon over the western North Pacific (5°–20°N, 110°–160°E)
ITCZ	Intertropical convergence zone
TUTT	Tropical upper tropospheric trough
MJO	Madden and Julian oscillation with a period of 30 to 90 days
ISO	Extratropical intraseasonal oscillation with a period of 30 to 90 days
BT	Barotropic mode as defined by averaging $\tilde{\zeta}$ at 850 and 200 hPa (Eq. (8))
BC	Baroclinic mode as defined by subtracting $\tilde{\zeta}$ at 850 hPa from that at 200 hPa (Eq. (8))

References

Chen, T.-C. and M. Murakami, 1988: The 30–50 day variation of convective activity over the western Pacific Ocean with emphasis on the northwestern region. *Mon. Wea. Rev.*, **116**, 892–906.

Ghil, M. and K. Mo, 1991: Intraseasonal oscillations in the global atmosphere. Part I: Northern Hemisphere and tropics. *J. Atmos. Sci.*, **48**, 752–779.

Gill, A.E., 1980: Some simple solutions for heat-induced tropical circulation. *Quart. J. Roy. Meteor. Soc.*, **106**, 447–462.

Goswami, B.N. and J. Shukla, 1984: Quasi-periodic oscillations in a symmetric general circulation model. *J. Atmos. Sci.*, **41**, 20–37.

Hayashi, Y.Y. and A. Sumi, 1986: The 30–40 day oscillations simulated in an "aqua-plane" model. *J. Meteor. Soc. Japan*, **64**, 451–467.

Hendon, H.H. and B. Liebmann, 1994: Organization of convection within the Madden-Julian oscillation. *J. Geophys. Res.*, **99**, 8073–8083.

Hendon, H.H. and M.L. Salby, 1994: The life cycle of the Madden-Julian oscillation. *J. Atmos. Sci.*, **51**, 2225–2237.

Holland, G.J., 1995: Scale interaction in the western Pacific monsoon. *Meteor. Atmos. Phys.*, **56**, 57–79.

Hoskins, B.J. and D.J. Karoly, 1981: The steady linear response of a spherical atmosphere to thermal and orographic forcing. *J. Atmos. Sci.*, **38**, 1179–1196.

Huang, R.H. and W.J. Li, 1987: Influence of the heat source anomaly over the western tropical Pacific on the subtropical high over East Asia. *Proc. International conference on the general circulation of East Asia*, 40–51.

Kawamura, R. and T. Murakami, 1995: Interaction between the mean summer monsoon flow and 45-day transient perturbations. *J. Meteor. Soc. Japan*, **73**, 1087–1114.

Knutson, T.R. and K.M. Weickmann, 1987: 30–60 day atmospheric oscillations: Composite life cycles of convection and circulation anomalies. *Mon. Wea. Rev.*, **115**, 1407–1436.

Krishnamurti, T.N. and D. Subrahmanyan, 1982: The 30–50 day mode at 850 mb during MONEX. *J. Atmos. Sci.*, **39**, 2088–2095.

Krishnamurti, T.N. and S. Gadgil, 1985: On the structure of the 30 to 50 day mode over the globe during FGGE. *Tellus*, **37**, 336–360.

Lau, K.-M. and P.H. Chan, 1986: Aspects of the 40–50 day oscillation during the northern summer as inferred from outgoing longwave radiation. *Mon. Wea. Rev.*, **114**, 1354–1367.

Lau, N.-C. and K.-M. Lau, 1986: The structure and propagation of intraseasonal oscillation appearing in a GFDL general circulation mode. *J. Atmos. Sci.*, **43**, 2023–2047.

Lau, N.-C., I.M. Held and J.D. Neelin, 1988: The Madden-Julian oscillation in an idealized general circulation model. *J. Atmos. Sci.*, **45**, 3810–3832.

Livezey, R.E and W.Y. Chen, 1983: Statistical field significance and its determination by Monte Carlo techniques. *Mon. Wea. Rev.*, **111**, 46–59.

Lorenc, A.C., 1984: The evolution of planetary scale 200 mb divergent flow during the FGGE year. *Quart. J. Roy. Meteor. Soc.*, **110**, 427–441.

Madden, R.A., 1986: Seasonal variations of the 40–50 day oscillation in the Tropics. *J. Atmos. Sci.*, **43**, 3138–3158.

Madden, R.A. and P.R. Julian, 1971: Detection of a 40–50 day oscillation in the zonal wind in the tropical Pacific. *J. Atmos. Sci.*, **28**, 702–708.

Madden, R.A. and P.R. Julian, 1972: Description of global-scale circulation cells in the tropics with a 40–50 day periods. *J. Atmos. Sci.*, **29**, 1109–1123.

Magana, V. and M. Yanai, 1991: Tropical-midlatitude interaction on the time scale of 30 to 60 days during the northern summer of 1979. *J. Climate*, **4**, 180–201.

Murakami, M., 1984: Analysis of the deep convective activity over the western Pacific and Southeast Asia. Part II: Seasonal and intraseasonal variations during northern summer. *J. Meteor. Soc. Japan*, **62**, 88–108.

Murakami, T., 1987: Intraseasonal atmospheric teleconnection patterns during the northern hemisphere summer. *Mon. Wea. Rev.*, **115**, 2133–2154.

Murakami, T. and T. Nakazawa, 1985: Tropical 45 day oscillations during the 1979 northern summer. *J. Atmos. Sci.*, **42**, 1107–1122.

Murakami, T. and J. Matsumoto, 1994: Summer monsoon over the Asian continent and the western North Pacific. *J. Meteor. Soc. Japan*, **72**, 719–745.

Murakami, T., T. Nakazawa and J.-H. He, 1984: On the 40–50 day oscillations during the 1979 northern hemisphere summer. Part I: Phase propagation. *J. Meteor. Soc. Japan*, **62**, 440–468.

Murakami, T., L.-X. Chen, A. Xie and M.L. Shrestha, 1986: Eastward propagation of 30–60 day perturbations as revealed from outgoing longwave radiation data. *J. Atmos. Sci.*, **43**, 961–971.

Nitta, T., 1987: Convective activities in the tropical western Pacific and their impact on the Northern Hemisphere summer circulation. *J. Meteor. Soc. Japan*, **65**, 373–390.

North, G.R., T.L. Bell and R.F. Cahalan, 1982: Sampling errors in the estimation of Empirical Orthogonal Function. *Mon. Wea. Rev.*, **110**, 669–706.

Panofsky, H.A. and G.W. Brier, 1958: *Some Applications of Statistics to Meteorology.* Pennsylvania State University, 219pp.

Sardeshmukh, P.D. and B.J. Hoskins, 1988: The generation of global rotational flow by steady idealized tropical divergence. *J. Atmos. Sci.*, **45**, 1228–1251.

Shanks, J.L., 1967: Recursion filters for digital processing. *Geophysica*, **32**, 33–51.

Sikka, D.R. and S. Gadgil, 1980: On the maximum cloud zone and the ITCZ over the Indian longitudes during the south-west monsoon. *Mon. Wea. Rev.*, **108**, 1840–1853.

Simmons, A.J., J.M. Wallace and G.W. Branstator, 1983: Barotropic wave propagation and instability, and atmospheric teleconnection patterns. *J. Atmos. Sci.*, **40**, 1363–1392.

Wang, B. and H. Rui, 1990: Synoptic climatology of transient tropical intraseasonal convection anomalies: 1975–1985. *Meteor. Atmos. Phys.*, **44**, 43–62.

Wang, B. and X. Xie, 1996: Low-frequency equatorial waves in vertically sheared zonal flow: Part I: Stable waves. *J. Atmos. Sci.*, **53**, 449–467.

Webster, P.J. and L. Chou, 1980: Low-frequency transitions of a simple monsoon system. *J. Atmos. Sci.*, **37**, 368–382.

Webster, P.J. and H.-R. Chang, 1988: Equatorial energy accumulation and emanation regions: Impacts of a zonally varying basic state. *J. Atmos. Sci.*, **45**, 803–829.

Yasunari, T., 1980: A quasi-stationary appearance of 30–40 day period in the cloudiness fluctuations during the summer monsoon over India. *J. Meteor. Soc. Japan*, **58**, 225–229.

Yasunari, T., 1981: Structure of an Indian summer monsoon system with a period around 40 days. *J. Meteor. Soc. Japan*, **59**, 336–354.

北半球夏季西部太平洋の熱帯・中緯度45日周期擾乱

川村隆一[1]・村上多喜雄・Bin Wang
(ハワイ大学気象学教室)

西太平洋モンスーン域(5°–20°N、110°–160°E)では熱帯Madden-Julian振動(MJO)は系統的に北へ伝播する。北進するMJOは水平的にも鉛直的にも非対称性の強い構造をもっている。対流圏下層の低気圧渦度は、低気圧シアーをもった収束性の平均モンスーン流の影響によって強い。一方、上層の高気圧渦度は、高気圧シアーをもった発散性の上層平均モンスーン流により弱くなる。対流圏上層の応答は顕著な赤道向きの発散風によって特徴づけられる。この発散風は南半球へ高気圧渦度を輸送する役割をもつ。夏季モンスーン循環は対流加熱によって誘因されたMJO循環の上下非対称性を強め、そのために、傾圧性の大きい発散性擾乱であるMJO内に順圧成分を生み出す効果がある。

中緯度45日周期擾乱(ISO)は北太平洋を横切る大円に沿った順圧的な波列パターンの一部として出現し、北太平洋の西風ジェットの出口付近(40°–50°N、180°–150°W)で最大振幅をもっている。この現象は、以下の二つの複合要因からもたらされる。MJOの北への伝播に伴って、モンスーンの効果で生成したMJOの順圧成分は季節内変動スケールの熱帯—中緯度相互作用を導く。すなわち、45日周期をもつ対流活動がフィリピン付近で極大になると、MJOの順圧成分が順圧ロスビー波の分散の起源として働き、中緯度における順圧渦的擾乱ISOの発達に寄与する。一方、エンストロフィー収支解析の結果から、西風ジェットの出口付近にみられるISOの強い変動度は主に平均流とISO擾乱との順圧相互作用に起因すると考えられる。